Phase retrieval and phaseless inverse scattering with background information

Thorsten Hohage, Roman Novikov, Vladimir Sivkin

Phase retrieval and phaseless inverse scattering with background information

by Thorsten Hohage, Roman G. Novikov & Vladimir N. Sivkin

November 17, 2022

Abstract. We consider the problem of finding a compactly supported potential in the multi-dimensional Schrödinger equation from its differential scattering cross section (squared modulus of the scattering amplitude) at fixed energy. In the Born approximation this problem simplifies to the phase retrieval problem of reconstructing the potential from the absolute value of its Fourier transform on a ball. To compensate for the missing phase information we use the method of a priori known background scatterers. In particular, we propose an iterative scheme for finding the potential from measurements of a single differential scattering cross section corresponding to the sum of the unknown potential and a known background potential, which is sufficiently disjoint. If this condition is relaxed, then we give similar results for finding the potential from additional monochromatic measurements of the differential scattering cross section of the unknown potential without the background potential. The performance of the proposed algorithms is demonstrated in numerical examples.

Keywords: Schrödinger equation, Helmholtz equation, monochromatic scattering, phaseless inverse scattering, phase retrieval problem, numerical reconstructions

AMS subject classification: 35J10, 35P25, 35R30, 65N21, 78A46, 81U40

1 Introduction

In this work we contribute to the study of phase retrieval problems and phaseless inverse scattering problems. These problems naturally arise in quantum mechanics, optics, and related areas such as electron tomography and X-ray imaging; see, for example, [20] and references therein. In particular, according to Born's rule in quantum mechanics complex (phased) values of a particle wave function have no direct physical interpretation, whereas their (phaseless) squared modulus admits a probabilistic interpretation and can be measured; see [9]. Similarly, in optics modern technical devices such as CCD cameras measure the intensity, i.e. the squared modulus, but it is very hard or impossible to measure the phase of time-harmonic electromagnetic waves in the frequency range of visible light or even X-rays.

In general, phase retrieval problems consist in finding a function $v : \mathbb{R}^d \to \mathbb{C}$ from the magnitude $|\widehat{v}|$ of its Fourier transform

$$\widehat{v}(p) = \mathcal{F}v(p) = \frac{1}{(2\pi)^d} \int_{\mathbb{R}^d} e^{ip\cdot x} v(x)\, dx, \tag{1.1}$$

often given only for p in some bounded subset of $\mathbb{R}^d$, e.g., $B_r := \{x \in \mathbb{R}^d : |x|_2 \leq r\}$. To compensate for the missing phase information $\widehat{v}/|\widehat{v}|$, one either assumes a-priori information on v or additional data. Such inversions of the Fourier transform from phaseless data are much more complicated than the inversion of the Fourier transform from phased data. Examples of a-priori informations include (approximate) knowledge of $\operatorname{supp} v$, constraints like $|v| = 1$ or $v \geq 0$, and knowledge of v on part of the domain. In this paper we will focus on the first and the last of these options. Such problems arise directly in phaseless linearized inverse scattering problems in quantum mechanics, optics and related areas such as electron tomography and X-ray imaging. We refer to the monographs [21, 7], the review papers [32, 39, 47], the article [12], and references therein.

We now give the precise formulation of the phase retrieval problems studied in this paper:

Problem 1. *(A) Reconstruct a function v from $|\widehat{v}+\widehat{w}|^2$ on B_R for some known function w under the a-priori assumption that* $\operatorname{supp} v$ *and* $\operatorname{supp} w$ *are compact and sufficiently separated.*

(B) Reconstruct v from $|\widehat{v}|^2$ and $|\widehat{v}+\widehat{w_j}|^2$, $j=1,\dots,n$, on B_R for some appropriate known functions $w_1,...,w_n$ separated from v.

Problem 1(B) was considered, in particular, in [36, 37, 1, 2]. In addition, related considerations go back, at least, to [43]. Problem 1(A) was studied in [41]. Other investigations related to this problem can be found in [44, 33]. In the present work we give, in particular, new mathematical and numerical results on Problem 1(A) and on Problem 1(B) for $n=1$.

Inverse scattering problems consist in finding functions describing a scattering object from data on scattered waves, usually at large distances from the scatterer. These problems are similar in many respects to reconstructing a function from its Fourier transform and, moreover, are reduced to such a Fourier inversion by the Born approximation, i.e. linearization around a zero background. Of course, also in situations where linearizations are not valid, only amplitudes can be measured for the same reasons as described above. This motivates the study of phaseless inverse scattering problems.

We consider the stationary Schrödinger equation of quantum mechanics:

$$-\Delta\psi+v(x)\psi=E\psi,\qquad x\in\mathbb{R}^d,\ d\geq 1,\ E>0, \tag{1.2}$$

where

$$v\in L^\infty(\mathbb{R}^d),\ \operatorname{supp} v\subset D,\ \ D\subset\mathbb{R}^d \text{ is open and bounded.} \tag{1.3}$$

Equation (1.2), under assumptions (1.3), arises in modelling interaction of a non-relativistic quantum mechanical particle at fixed energy E with a macroscopic object contained in D, where v is the potential of this interaction. Here, we assume that $\hbar^2/(2m)=1$, where $\hbar$ is the reduced Planck's constant, and m is the mass of the particle. For more details on such a model in the framework of electron tomography, see, for example, [15].

We also consider the time harmonic Helmholtz equation of electrodynamics and acoustics:

$$\Delta\psi+\kappa^2n^2(x)\psi=0,\qquad \kappa=\omega/c_0, \tag{1.4}$$

where ω is the frequency, c_0 is a reference speed of wave propagation, $n(x)$ is a scalar index of refraction, $n(x)\equiv 1$ for $x\in\mathbb{R}^d\setminus D$, and D is as in (1.3). We recall that in the simplest case $n(x)=c_0/c(x)$, where $c(x)$ is a speed of wave propagation. For more details on such a model in the framework of X-ray imaging, see, for example, [49]. We recall that the Helmholtz equation (1.4) at fixed ω can be written in the form of the Schrödinger equation (1.2), (1.3), where

$$v(x)=(1-n^2(x))E,\quad E=\left(\frac{\omega}{c_0}\right)^2. \tag{1.5}$$

For equation (1.2), under condition (1.3), we consider the scattering solutions $\psi^+=\psi^+(x,k)$, $k\in\mathbb{R}^d$, $k^2=E$, specified by the conditions

$$\psi^+(x,k)=e^{ikx}+\psi^{\rm sc}(x,k); \tag{1.6}$$

$$|x|^{(d-1)/2}\left(\frac{\partial}{\partial|x|}-i|k|\right)\psi^{\rm sc}(x,k)\to 0\ \text{ as } |x|\to+\infty, \tag{1.7}$$

uniformly in $x/|x|$. The Sommerfeld radiation condition (1.7) implies that

$$\psi^{\rm sc}(x,k)=\frac{e^{i|k||x|}}{|x|^{(d-1)/2}}A\left(k,|k|\frac{x}{|x|}\right)+O\left(\frac{1}{|x|^{(d+1)/2}}\right)\quad \text{as } |x|\to+\infty, \tag{1.8}$$

where $A=A[v]$ is the scattering amplitude for equation (1.2). For more information on the definitions of ψ^+ and A, see, for example, [8], [39] and references therein.

In turn, $\sigma[v](k,l) = |A[v](k,l)|^2$ is known as the differential scattering cross section for equation (1.2). We will suppress v in $\sigma[v]$ and $A[v]$ if there is no ambiguity. As for particle wave functions, A admits no direct physical interpretation whereas $|A|^2$ is the expected value of quantities that can be measured in experiments; see, for example, [9], [16]. In particular, the differential scattering cross section $\sigma(k,l)$ describes the probability density of scattering of a particle with initial impulse k into direction $l/|l| \neq k/|k|$. Similarly, in the electromagnetism of optics and X-rays only $|\psi^+|^2$ and $\sigma = |A|^2$ can be measured directly by modern technical devices.

Note that the aforementioned functions A and $\sigma = |A|^2$ are defined on

$$\mathcal{M}_E = \{k,\, l \in \mathbb{R}^d : \quad k^2 = l^2 = E\} = \mathbb{S}^{d-1}_{\sqrt{E}} \times \mathbb{S}^{d-1}_{\sqrt{E}}. \tag{1.9}$$

We consider the following monochromatic phaseless inverse scattering problems which reduce to Problem 1 in the Born approximation:

Problem 2. *(A) Reconstruct a compactly supported potential v in (1.2) from the differential scattering cross section $\sigma[v+w]$ on some appropriate $\mathcal{M}' \subseteq \mathcal{M}_E$ for some known compactly supported background potential w sufficiently separated from v.*

(B) Reconstruct v from $\sigma[v]$ and $\sigma[v+w_j]$, $j = 1, \dots, n$ on some appropriate $\mathcal{M}' \subseteq \mathcal{M}_E$ (see (1.9)) for some appropriate known background potentials $w_1, ..., w_n$ separated from v.

Phaseless inverse scattering problems are much more difficult than usual inverse scattering problems with phase information, and until recently very little results have been known for such problems (see, e.g., [1, 11, 39, 41] and references therein). In particular, it is well known that $\sigma = |A|^2$ on $\mathcal{M}_{\mathbb{R}_+} = \bigcup_{E \in \mathbb{R}_+} \mathcal{M}_E$ does not determine v uniquely, in general; see, for example, [39].

In addition to Problem 2 there are also other possible formulations of phaseless inverse scattering problems for equation (1.2) and for other equations of wave propagation. In connection with such formulations and related results, see, for example, [5], [11], [17], [20], [22], [23], [27], [29]–[31], [36], [38]–[40], [42], [45], [46], [52], [53] and references therein.

Following previous works of the authors, our general approach for "solving" Problems 1 and 2 is to provide explicit reconstruction formulas only for the stable part of the solution defined roughly in terms of the classical diffraction limit. These reconstruction formulas only provide a smoothed version of the unknown function v. They do not converge to the true solution v as the noise level tends to zero, but only as the energy (or wave number) tends to infinity. On the other hand, in contrast to regularization methods, they are Lipschitz stable with respect to data noise, they do not require a sufficiently good initial guess, and they are cheaper to compute. For small noise levels, our reconstructions can be improved by using them as initial guess for iterative regularization methods. Probably, our reconstructions can be also improved using the approach of [26], but this issue requires additional studies.

Our main results can be summarized as follows:

We propose an iterative reconstruction algorithm for Problem 2(A) in dimension $d \geq 2$ under the condition that $\operatorname{supp} v$ and $\operatorname{supp} w$ are sufficiently disjoint. If this condition is relaxed, then we give similar results just for Problem 2(B) with $d \geq 2$ and $n = 1$. This iterative monochromatic reconstruction is analogous to the algorithm suggested in [35] for inverse scattering problems with phase information at fixed sufficiently large energy E. This reconstruction is considerably simpler than the algorithm developed in [1] for Problem 2(B) with $d \geq 2$ and $n = 2$. This reconstruction proceeds from results of [41], which provide, in particular, the first approximation. In addition, for our iterates u^j_E, $j = 1, 2, ...$, we have that

$$\|v - u^j_E\|_{L^\infty} = \mathcal{O}(E^{-\alpha_j}) \text{ as } E \to +\infty, \tag{1.10}$$

with α_j tending to $+\infty$ as $j \to \infty$, for infinitely smooth v. See Section 3.2.

We implement numerically the aforementioned iterative monochromatic reconstruction, at least, for $d = 2$; see Sections 4 and 5.

In connection with the aforementioned monochromatic reconstruction v_E in the Born approximation our study also includes new results on Problem 1(A) and Problem 1(B) for $n = 1$. In particular, in this case proceeding from [41] we show that

$$\|v - v_E\|_{L^\infty} = \mathcal{O}(E^{-\alpha}) \text{ as } E \to +\infty,\ \alpha = \frac{1}{2}(m-d), \tag{1.11}$$

where v is m-times smooth in $L^1(\mathbb{R}^d)$; see Section 3.1. Note that estimate (1.11) is an analog for the phaseless case of estimate (2.16) for the phased case. In addition, in numerical reconstruction of v_E from the data on discrete Ewald grid in $B_{2\sqrt{E}}$, we modified the related conjugate gradient approach of [1]; see Section 4.3.

The further structure of the present article is as follows. In Section 2 we recall some known results on direct and inverse scattering for equation (1.2) under assumptions (1.3), including results on Problems 1 and 2. Our main new theoretical results on Problems 1 and 2 are given in Section 3. Our numerical results on these problems are presented in Sections 4, 5. In conclusion, we discuss the results of the present work, previous results, and natural further research directions; see Section 6. Some proofs are also given in Sections A and B of Appendix.

2 Preliminaries

2.1 Direct scattering

For equation (1.2), under condition (1.3), we consider the scattered field ψ^+, its scattering amplitude A, and its scattering cross section $\sigma = |A|^2$ mentioned in the Introduction; see formulas (1.6), (1.7), and (1.8). For finding these functions from v one can use the Lippmann-Schwinger integral equation

$$\begin{aligned} \psi^+(x,k) &= e^{ikx} + \int_{\mathbb{R}^d} G^+(x-y,k)v(y)\psi^+(y,k)dy, \\ G^+(x,k) &= -(2\pi)^{-d}\int_{\mathbb{R}^d} \frac{e^{i\xi x}d\xi}{\xi^2 - k^2 - i0} = G_0^+(|x|,|k|,d), \end{aligned} \tag{2.1}$$

for ψ^+ with $x,\ k \in \mathbb{R}^d$, $k^2 = E$ and the following formulas for A:

$$\begin{aligned} &A(k,l) := c(d,|k|)f(k,l),\ (k,l) \in \mathcal{M}_E, \\ &c(d,|k|) := -\pi i(-2\pi i)^{(d-1)/2}|k|^{(d-3)/2},\ \text{for } \sqrt{-2\pi i} = \sqrt{2\pi}e^{-i\pi/4}, \end{aligned} \tag{2.2a}$$

$$f(k,l) := (2\pi)^{-d}\int_{\mathbb{R}^d} e^{-ily}v(y)\psi^+(y,k)dy, \tag{2.2b}$$

We will use the term 'scattering amplitude' also for f arising in (2.2).

Note that one can also use equation (2.1) and formula (2.2b) for the case when

$$v \in L^\infty_s(\mathbb{R}^d),\ \text{ for some } s > d, \tag{2.3}$$

where

$$L^\infty_s(\mathbb{R}^d) = \{u \in L^\infty(\mathbb{R}^d) : \|u\|_s < \infty\}, \tag{2.4}$$

$$\|u\|_s = \operatorname{ess\,sup}_{\mathbb{R}^d}(1+|x|^2)^{s/2}|u(x)|,\ s \geq 0; \tag{2.5}$$

see, for example, [8], [39] and references therein.

Let

$$B_r = \{x \in \mathbb{R}^d : |x| \leq r\}. \tag{2.6}$$

In addition to A, σ, and f on $\mathcal{M}_E$, we also consider their restrictions to lower-dimensional subsets $\Gamma_E \subset \mathcal{M}_E$ for which the function

$$\tilde{\Phi} : \Gamma_E \to B_{2\sqrt{E}}, \qquad \tilde{\Phi}(k,l) := k - l \tag{2.7}$$

is surjective, where B_r is defined by (2.6), $d \geq 2$; see [1]. In particular, $\tilde{\Phi}$ is bijective if Γ_E is defined as in [35]:

$$\begin{aligned} &\Gamma_E = \left\{k = k_E(p),\, l = l_E(p) \,:\, p \in B_{2\sqrt{E}}\right\}, \\ &k_E(p) = p/2 + (E - p^2/4)^{1/2}\gamma(p),\ l_E(p) = -p/2 + (E - p^2/4)^{1/2}\gamma(p), \end{aligned} \tag{2.8}$$

where γ is a piecewise continuous vector–function on $\mathbb{R}^d$, $d \geq 2$, such that

$$|\gamma(p)| = 1,\ \gamma(p)p = 0,\ p \in \mathbb{R}^d. \tag{2.9}$$

In general we assume that for each $p \in B_{2\sqrt{E}}$ the set $\tilde{\Phi}^{-1}(p)$ is a piecewise smooth manifold of size $|\tilde{\Phi}^{-1}(p)|$ and define the averaging operator

$$(\Phi f)(p) := \frac{1}{|\tilde{\Phi}^{-1}(p)|} \int_{\tilde{\Phi}^{-1}(p)} f(k,l)d(k,l),\ \ p \in B_{2\sqrt{E}}. \tag{2.10}$$

Note that if Γ_E is defined by (2.8), then

$$(\Phi f)(p) = f(k_E(p), l_E(p)),\ p \in B_{2\sqrt{E}}. \tag{2.11}$$

To deal with equation (2.1) at large E, it is convenient to use the following Agmon estimate

$$\|\langle x\rangle^{-s}\mathcal{G}_0^+(E)\langle x\rangle^{-s}\|_{L^2(\mathbb{R}^d)\to L^2(\mathbb{R}^d)} \leq a_0(d,s)E^{-1/2},\ E \geq 1,\ s > 1/2, \tag{2.12}$$

where $\langle x\rangle$ denotes the multiplication operator by the function $(1+|x|^2)^{1/2}$, and $\mathcal{G}_0^+(E) : L^2(\mathbb{R}^d) \to L^2(\mathbb{R}^d)$ denotes the integral operator

$$\mathcal{G}_0^+(E)u(x) := \int_{\mathbb{R}^d} G_0^+(|x-y|, \sqrt{E}, d)u(y)dy, \tag{2.13}$$

with kernel $G_0^+(|x|, \sqrt{E}, d)$ defined in (2.1); see, for example, [13], [35].

2.2 Some known results on inverse scattering problems with phase information

We recall that in the Born approximation for small v, for $d \geq 2$, the scattering amplitude f on Γ_E (and on $\mathcal{M}_E$) reduces to the Fourier transform $\widehat{v}$ on $B_{2\sqrt{E}}$ via the formula

$$f(k,l) \approx \widehat{v}(p),\ (k,l) \in \mathcal{M}_E,\ p = k - l, \tag{2.14}$$

where f is defined by (2.2), $\widehat{v}$ is defined by (1.1).

Moreover, for u_E defined by

$$u_E(x) := \int_{B_{2\sqrt{E}}} e^{-ipx}\widehat{v}(p)dp, \tag{2.15}$$

we have that

$$\|v - u_E\|_{L^\infty(\mathbb{R}^d)} = \mathcal{O}(E^{-\alpha}) \text{ as } E \to +\infty \text{ with } \alpha := \frac{1}{2}(m-d), \tag{2.16}$$

where v is m-times smooth in $L^1(\mathbb{R}^d)$. For more details on the linearised monochromatic reconstruction u_E, see, for example, [39].

Besides, in general (i.e., without assumption that v is small), for finding $\widehat{v}$ from f on Γ_E at large E, for $d \geq 2$, one can use the following formulas:

$$\widehat{v}(p) = f(k,l) + \mathcal{O}(E^{-1/2}) \ \text{ as } \ E \to +\infty,\ \ (k,l) \in \mathcal{M}_E,\ \ k - l = p \in \mathbb{R}^d, \tag{2.17}$$

$$\begin{aligned} &|f(k,l) - \widehat{v}(k-l)| \leq (2\pi)^{-d}a_0(d,s/2)(c_1(d,s)\|v\|_s)^2E^{-1/2}, \\ &E^{1/2} \geq \rho_1(d,s,\|v\|_s),\ (k,l) \in \mathcal{M}_E,\ s > d. \end{aligned} \tag{2.18}$$

Here $a_0(d, s/2)$ is defined in (2.12) and

$$c_1(d,s) := \left(\int_{\mathbb{R}^d} \frac{dx}{(1+|x|^2)^{s/2}} \right)^{1/2}, \tag{2.19}$$

$$\rho_1(d,s,N) := \max\left(2a_0(d,s/2)N, 1\right). \tag{2.20}$$

Formula (2.17) goes back to [14] and can be considered as Born approximation for f at higher energies. In connection with estimate (2.18), see, for example, [35].

In turn, estimate (2.18) can be considered as particular case of the following important lemma.

Lemma 2.1. *([35]). Let v satisfy (2.3), D be bounded domain in $\mathbb{R}^d$, f be the scattering amplitude for v, and $v_{\rm appr}(\cdot, E)$ be an approximation to v such that:*

$$|v_{\rm appr}(x,E) - v(x)| \le bE^{-\alpha}, \qquad x \in D,\ \sqrt{E} \ge \rho_1(d,s,N), \tag{2.21}$$

$$v_{\rm appr}(x,E) = v(x), \qquad x \in \mathbb{R}^d \setminus D, \tag{2.22}$$

for some α, $b > 0$, and some N such that

$$\|v\|_s \le N, \quad \|v_{\rm appr}(\cdot,E)\|_s \le N, \quad \sqrt{E} \ge \rho_1(d,s,N). \tag{2.23}$$

Then the following estimate holds:

$$|f(k,l) - f_{\rm appr}(k,l) + \widehat{v}_{\rm appr}(k-l,E) - \widehat{v}(k-l)| \le \frac{Nb}{(2\pi)^d} a_0(d,\tfrac{s}{2}) c_1(d,s) c_2(D,s) E^{-\alpha-\frac{1}{2}}, \quad (k,l) \in \mathcal{M}_E,\ E^{1/2} \ge \rho_1(d,s,N), \tag{2.24}$$

where $f_{\rm appr}$ is the scattering amplitude for $v_{\rm appr}(\cdot,E)$, $\widehat{v}$ is the Fourier transform of v, $\widehat{v}_{\rm appr}(\cdot,E)$ is the Fourier transform of $v_{\rm appr}(\cdot,E)$,

$$c_2(D,s) = 2\|\Lambda^{s/2}\|_{L^2(D)} + 4\|\Lambda^{-s/2}\|_{L^2(\mathbb{R}^d)} \|\Lambda^s\|_{L^\infty(D)}, \tag{2.25}$$

$$\Lambda = (1+|x|^2)^{1/2}. \tag{2.26}$$

Suppose that

$$v - v_0 \in W^{m,1}(\mathbb{R}^d),\ \mathrm{supp}(v-v_0) \subset D,\ v_0 \text{ satisfies (2.3)}, \tag{2.27}$$

with the Sobolev space

$$W^{m,1}(\mathbb{R}^d) := \{u : \partial^J u \in L^1(\mathbb{R}^d),\ |J| \le m\},$$
$$\|u\|_{m,1} := \max_{|J|\le m} \|\partial^J u\|_{L^1(\mathbb{R}^d)},\ m \in \mathbb{N} \cup 0. \tag{2.28}$$

Using estimate (2.18) and Lemma 2.1, under conditions (2.27), work [35] constructs the iterates u_E^j from f on Γ_E such that

$$\|v - u_E^j\|_{L^\infty(D)} = \mathcal{O}(E^{-\alpha_j}) \ \text{ as } E \to +\infty \text{ with} \tag{2.29}$$

$$\alpha_1 := \frac{m-d}{2m},\ \ \alpha_j := \left(1 - \left(\frac{m-d}{m}\right)^j\right) \frac{m-d}{2d},\ j \ge 1. \tag{2.30}$$

More precisely, this construction of u_E^j is based on formula (2.18), if $j = 1$, and uses iteratively Lemma 2.1, if $j > 1$. In addition, one can see that

$$\begin{aligned} &\alpha_j \to \alpha_\infty := \frac{m-d}{2d} && \text{as } j \to +\infty, \\ &\alpha_j \to \frac{j}{2} && \text{as } m \to +\infty, \\ &\alpha_\infty \to +\infty && \text{as } m \to +\infty. \end{aligned} \tag{2.31}$$

Therefore, the convergence in (2.29), as $E \to +\infty$, is drastically better for $j > 1$ than for $j = 1$, at least, for large m and j.

The iterative monochromatic reconstruction of [35] is implemented numerically in [6], [48] for $d = 2$. For other monochromatic phased inverse scattering reconstructions for equations (1.2) and (1.4), see, for example, [4], [10], [18], [39].

2.3 Some known results on Problems 1 and 2

In addition to v satisfying (1.3), we consider a priori known background scatterers $w_1, ..., w_n$ such that

$$\begin{aligned} &w_j \in L^\infty(\mathbb{R}^d),\ \ w_j \neq 0 \text{ in } L^\infty(\mathbb{R}^d), \quad \operatorname{supp} w_j \subset \Omega_j, \\ &\Omega_j \ \text{ is an open bounded domain in } \ \mathbb{R}^d,\ \Omega_j \cap D = \varnothing, \\ &w_{j_1} \neq w_{j_2} \ \text{ for } \ j_1 \neq j_2 \ \text{ in } \ L^\infty(\mathbb{R}^d), \\ &j,\ j_1,\ j_2 \in \{1, \dots, n\}. \end{aligned} \tag{2.32}$$

Under assumptions (1.3), (2.32), $d \geq 2$, we have that

$$|\widehat{v}_j(p)|^2 = |f_j(k,l)|^2 + \mathcal{O}(E^{-1/2}) \text{ as } E \to +\infty,\ (k,l) \in \mathcal{M}_E,\ k - l = p \in \mathbb{R}^d,\ j = 0, 1, ..., \tag{2.33}$$

where $v_0 = v$, $v_j = v + w_j$, $j \geq 1$, f_j is related to A_j according to (2.2a) and is the scattering amplitude for v_j.

In addition, for small v and w_j, we have that

$$|\widehat{v}_j(p)|^2 \approx |f_j(k,l)|^2,\ p = k - l,\ k - l \in \mathcal{M}_E. \tag{2.34}$$

Formulas (2.33), (2.34) are phaseless versions of (2.17), (2.14); for phaseless version of (2.18), see, for example, [37]. These formulas reduce Problems 2 to Problem 1.

For open bounded domains D, Ω_1, $\mathcal{U} \subset \mathbb{R}^d$ and $\varepsilon > 0$ we introduce the following notation:

$$D - \Omega_1 := \{x - y :\ x \in D,\ y \in \Omega_1\}, \tag{2.35a}$$

$$\operatorname{dist}(D, \Omega_1) := \inf_{x \in D,\, y \in \Omega_1} |x - y|, \quad \operatorname{diam} D := \sup_{x,\, y \in D} |x - y|, \tag{2.35b}$$

$$\chi_{\mathcal{U},\varepsilon} \in C^\infty(\mathbb{R}^d),\ 0 \leq \chi_{\mathcal{U},\varepsilon} \leq 1, \tag{2.35c}$$

$$\chi_{\mathcal{U},\varepsilon}(x) := \begin{cases} 1,\ x \in \mathcal{U}, \\ 0,\ \operatorname{dist}(x, \mathcal{U}) > \varepsilon \end{cases} \tag{2.35d}$$

The recent work [41] defines an approximate reconstruction v_E of the unknown potential v for Problems 2(A) and 2(B, $n = 1$) with $d \geq 2$, convex D and Ω_1, and $\mathcal{M}' = \Gamma_E$. In case of Problem 2(A) with scattering data $\sigma_1 = \sigma[v + w_1]$ on Γ_E, it is assumed that $\operatorname{dist}(D, \Omega_1) > \operatorname{diam} D$, whereas for Problem 2(B, $n = 1$) with scattering data $\{\sigma, \sigma_1\} = \{\sigma[v], \sigma[v + w_1]\}$ on Γ_E only $\operatorname{dist}(D, \Omega_1) > 0$ is required. The reconstruction v_E is defined by Algorithm 1 with $\nu = 1$ in [41] and Q_E given by

$$Q_E(p) := \tfrac{1}{|c(d, \sqrt{E})|^2}(\Phi\sigma_1)(p), \qquad p \in B_{2\sqrt{E}}, \quad \text{for Problem 2(A)}, \tag{2.36a}$$

$$Q_E(p) := \tfrac{1}{|c(d, \sqrt{E})|^2}((\Phi\sigma_1)(p) - (\Phi\sigma)(p)), \qquad p \in B_{2\sqrt{E}}, \quad \text{for Problem 2(B, } n = 1), \tag{2.36b}$$

where $c(d, \sqrt{E})$ is given by (2.2a).

Algorithm 1: function $v_E = \texttt{reco}(Q_E, w, E, D, \nu, \tau)$

// basic reconstruction procedure proposed in [41]; see also Alg. 3 for a discrete version

Input:

Q_E: is computed from data by (2.39) for Problem 1 and by (2.36) for Problem 2

$w \in L^\infty(\mathbb{R}^d)$: background potential

$E > 0$: energy

convex $D \subset \mathbb{R}^d$ contains $\operatorname{supp} v$ for unknown function v

$\nu, \tau \in (0, 1]$: cut-off parameters

Output:

v_E: approximation of unknown function v

1 $h_E(p) := \begin{cases} Q_E(p), & p \in B_{2\nu\sqrt{E}} \\ |\mathcal{F}w_1(p)|^2, & p \in \mathbb{R}^d \setminus B_{2\nu\sqrt{E}} \end{cases}$

2 Set $\Omega \subset \mathbb{R}^d$ as convex hull of $\operatorname{supp} w$

3 $W(x) := (2\pi)^{-d} \int_\Omega w(x+y)\overline{w(y)}\, dy$

4 $q_E(x) := \chi_{D-\Omega,\varepsilon}(x)((\mathcal{F}^{-1}h_E)(x) - W(x))$

// cut-off function $\chi_{D-\Omega,\varepsilon}$ defined in (2.35c), Fourier transform $\mathcal{F}$ in (1.1)

5 $\widehat{v}_E(p) := \begin{cases} (\overline{\mathcal{F}w(p)})^{-1}(\mathcal{F}q_E)(p), & p \in B_{2\tau\sqrt{E}} \\ 0, & p \in \mathbb{R}^d \setminus B_{2\tau\sqrt{E}} \end{cases}$

6 $v_E(x) := \begin{cases} (\mathcal{F}^{-1}\widehat{v}_E)(x), & x \in D \\ 0, & x \in \mathbb{R}^d \setminus D \end{cases}$

Results of [41] include estimates on $\widehat{v} - \widehat{v}_E$ and $v - v_E$. In particular, suppose also that in Algorithm 1, where Q_E is given by (2.36) and $\nu = 1$, the potentials v, $w = w_1$ and the parameter τ are such that

$$v \in W^{m,1}(\mathbb{R}^d), \quad m > d, \tag{2.37a}$$

$$\max(\|v\|_{L^\infty(D)}, \|w_1\|_{L^\infty(\Omega_1)}) \le \eta, \tag{2.37b}$$

$$\|v + w_1\|_s \le N, \quad s > d, \tag{2.37c}$$

$$|(\mathcal{F}w_1)(p)| \ge c_3(1 + |p|)^{-\beta}, \ \forall\, p \in \mathbb{R}^d, \ \beta > d, \ c_3 > 0, \tag{2.37d}$$

$$\tau_1 = \tau_1(E) = \tau E^{\gamma - 1/2}, \quad 0 < \tau < 1, \quad \gamma = \frac{1}{2}\frac{1}{m+\beta}; \tag{2.37e}$$

see [41] (and also [2] in connection with condition (2.37d)). Then we have that ([41]):

$$|v(x) - v_E(x)| \le \left(C_1(m, d, \tau)\|v\|_{m,1} + C_2(\beta, \tau, d, D, \Omega_1)\frac{\eta^2}{c_3} + C_3(\beta, d, \tau, D, \Omega_1, \varepsilon)\frac{\eta^3}{c_3} \right) E^{-\alpha_1},$$
$$x \in D, \quad \sqrt{E} \ge \rho_1(d, s, N), \quad \alpha_1 = \frac{1}{2}\frac{m-d}{m+\beta}. \tag{2.38}$$

Explicit expressions for C_1, C_2, C_3 are given in [41] (with misprint c_3 in place of correct c_3^{-1}).

For small v and w_1, the function v_E given by (2.36) and lines 1–6 of Alg. 1 reduces to an approximate reconstruction for the case of Problems 1(A) and 1(B, $n = 1$) with $d \ge 2$, convex D and Ω_1, $B = B_{2\sqrt{E}}$.

In addition, for Problem 1, we use Algorithm 1, where

$$Q_E(p) := |\mathcal{F}(v + w_1)(p)|^2, \qquad p \in B_{2\sqrt{E}}, \quad \text{for Problem 2(A)}, \tag{2.39a}$$

$$Q_E(p) := |\mathcal{F}(v + w_1)(p)|^2 - |\mathcal{F}(v)(p)|^2, \qquad p \in B_{2\sqrt{E}}, \quad \text{for Problem 2(B, } n = 1), \tag{2.39b}$$

$\operatorname{dist}(D, \Omega_1) > \operatorname{diam} D$ for the case (A), and $\operatorname{dist}(D, \Omega_1) > 0$ for the case (B, $n = 1$).

In addition,

$$v_E \to v \text{ on } D \text{ as } E \to +\infty. \tag{2.40}$$

For example, under the additional assumptions (2.37a), (2.37d), (2.37e), we have that:

$$\|v - v_E\|_{L^\infty(D)} = \mathcal{O}(E^{-\alpha_1}) \text{ as } E \to +\infty \text{ with } \alpha_1 := \frac{1}{2}\frac{m-d}{m+\beta}. \tag{2.41}$$

3 Main new theoretical results

3.1 The case of Problem 1

For Problems 1(A) and 1(B, $n = 1$) with $d \geq 2$, convex D and Ω_1, and $B = B_{2\sqrt{E}}$, we consider the approximate reconstruction v_E defined by Algorithm 1 with Q_E given by (2.39).

We will use that

$$|\mathcal{F}\chi_{D-\Omega_1,\varepsilon}(p)| \leq \frac{C_4(t)}{(1+|p|)^t}, \quad p \in \mathbb{R}^d,\, t \geq 0, \tag{3.1}$$

where $\chi_{D-\Omega_1,\varepsilon}$ is the function in line 4 of Alg. 1, $C_4(t) = C_4(t, \chi_{D-\Omega_1,\varepsilon})$ is a positive constant.

Let

$$C_5(t) := \int_{\mathbb{R}^d} \frac{dp}{(1+|p|)^t}, \quad t > d. \tag{3.2}$$

Let $\mu(\mathcal{U})$ denote the Lebesgue measure of a bounded domain $\mathcal{U} \subset \mathbb{R}^d$.

We give the following new estimate on $\widehat{v}_E = \mathcal{F}v_E$ on $B_{2\sqrt{E}}$.

Proposition 3.1. *Let v, w_1 satisfy (1.3), (2.32), (2.37b), where D, Ω_1 are convex, and* $\operatorname{dist}(D, \Omega_1) > \operatorname{diam} D$. *Let $\widehat{v}_E$ be defined via* (2.39a)*) and lines 1–5 of Alg. 1, where $\nu = 1$. Then:*

$$|\widehat{v}(p) - \widehat{v}_E(p)| \leq \frac{C_6\eta^2}{|\mathcal{F}w_1(p)|(1+2(1-\tau)E^{1/2})^{t-d-\alpha}}, \quad p \in B_{2\tau\sqrt{E}},\ E^{1/2} \geq \rho_1(d, s, \|v+w_1\|_s), \tag{3.3}$$

$$C_6 := (2\pi)^{-2d}(\mu(D)^2 + 2\mu(D)\mu(\Omega_1))C_4(t)C_5(d+\delta), \quad \delta > 0,\, t-d-\delta > 0, \tag{3.4}$$

where ρ_1 is defined by (2.20), C_4, C_5 are the constants of (3.1), (3.2), *$\tau \in (0,1)$ is the parameter in line 5 of Alg. 1 and is fixed.*

The proof of Proposition 3.1 repeats the proof of Theorem 5.1 (for Problem 2(A)) in [41]. The main difference is that now formulas (114), (122) in [41] reduce to

$$\Delta h(p, E) = 0 \quad \text{for } p \in B_{2\sqrt{E}}, \tag{3.5}$$

$$I_1(p, E) = 0. \tag{3.6}$$

Actually, this completes the proof of Proposition 3.1.

Recall that if $v \in W^{m,1}(\mathbb{R}^d)$, $m \geq 0$, then the following estimate holds:

$$|\widehat{v}(p)| \leq \frac{C_7(m)}{(1+|p|)^m}, \quad p \in \mathbb{R}^d, \tag{3.7}$$

where $C_7(m) = C_7(m, d, \|v\|_{m,1})$ is positive constant.

Let $|\mathbb{S}^{d-1}|$ denote the $(d-1)$–dimensional Lebesgue measure of the unit sphere.

Proposition 3.1 and estimate (3.7) yield the following new estimate on v_E on D.

Theorem 3.2. *Let v, w_1 satisfy the assumptions of Proposition 3.1, and also satisfy (2.37a) and (2.37d). Let v_E be defined by Algorithm 1 with Q_E given by (2.39a) and $\nu = 1$. Let $\delta > 0$, $t - \beta - \delta > 2d$. Then:*

$$|v(x) - v_E(x)| \le A_1 E^{-\alpha_1} + A_2 E^{-\alpha_2},\ x \in D, \tag{3.8a}$$

$$\alpha_1 := \frac{1}{2}(m-d), \quad \alpha_2 := \frac{t-\beta-\delta}{2} - d, \tag{3.8b}$$

$$A_1 := \frac{|\mathbb{S}^{d-1}| C_7(m)}{(2\tau)^{m-d}(m-d)}, \tag{3.8c}$$

$$A_2 := \frac{(1+2\tau)^\beta (2\tau)^\beta}{(2-2\tau)^{t-d-\delta}} \mu(B_1) c_3^{-1} C_6(t) \eta^2, \tag{3.8d}$$

where C_6, C_7 are given by (3.4), (3.7), and $\tau \in (0,1)$, the parameter in line 5 of Alg. 1 is fixed.

The proof of Theorem 3.2 repeats the proof of Theorem 6.1 (for Problem 2(A)) in [41]. The main modifications consist in the following:

- In formula (136) of [41]: $\gamma = 1/2$, i.e., $\tau_1 = \tau$ is independent of E;
- In formula (139) of [41]: $I_1 = 0$.

Remark 3.3. *For Problem 1(B, $n = 1$), where* $\operatorname{dist}(D, \Omega_1) > 0$, *Proposition 3.1 and Theorem 3.2 are valid with Q_E given by (2.39b) and C_6 given by*

$$C_6 = 2(2\pi)^{-2d} \mu(D) \mu(\Omega_1) C_4(t) C_5(d+\delta).$$

Remark 3.4. *Estimate (3.8a) (with t such that $\alpha_2 = \alpha_1$) implies estimate (1.11) mentioned in Introduction. The point is that estimate (1.11) is completely similar to estimate (2.16) for the phased case and is principally better than estimate (2.41) for the phaseless case. Note that v_E in (2.41) is constructed with different τ than v_E in (3.8a), (1.11).*

Remark 3.5. *If the assumption that $v \in W^{m,1}(\mathbb{R}^d)$, $m > d$, is not fulfilled, then the result of Theorem 3.1 can be modified for apodized (smoothed) v in a similar way with considerations of Section 6.1 of [24] and Theorem 3.2, Remark 3.3 of [25].*

3.2 The case of Problem 2

For Problems 2(A) and 2(B, $n = 1$) with $d \ge 2$, convex D and Ω_1, and $\mathcal{M}' = \Gamma_E$, the approximate reconstruction v_E given by Algorithm 1 can be essentially improved iteratively, where $u_E^1 = v_E$ is the first approximation.

The iterative step is based on the following lemma.

Lemma 3.6. *Under the assumptions of Lemma 2.1, the following estimate holds:*

$$\left| |f(k,l)|^2 - |f_{\text{appr}}(k,l)|^2 + |\widehat{v}_{\text{appr}}(k-l,E)|^2 - |\widehat{v}(k-l)|^2 \right| \le C(s,D) \left(N + \tfrac{b}{E^\alpha} \left(1 + \tfrac{N}{E^{1/2}} \right) \right) \frac{Nb}{E^{\alpha+1/2}},$$
$$(k,l) \in \mathcal{M}_E, \quad E^{1/2} \ge \rho_1(d,s,N), \tag{3.9}$$

for some $C = C(s,D) > 0$.

The proof of Lemma 3.6 is given in Section A.

Our iterative reconstruction is summarized in Algorithms 2(A) and 2(B).

Algorithm 2(A): function $u_E^J = \texttt{reco2A}(\sigma_1, w, E, \{\nu_1..\nu_J\}, \{\tau_1..\tau_J\}, D)$
// iterative reconstruction algorithm for Problem 2(A)

Input:
$\sigma_1 \approx \sigma[v+w]$: measured scattering cross section for $v+w$ on $\mathcal{M}'$
$w \in L^\infty(\mathbb{R}^d)$: background potential
$E > 0$: energy
$0 < \nu_1 \le \cdots \le \nu_J \le 1$: cut-off parameters
$0 < \tau_1 \le \cdots \le \tau_J \le 1$: cut-off parameters
convex $D \subset \mathbb{R}^d$ contains $\operatorname{supp} v$

Output:
u_E^J: approximate reconstruction of v

$Q_E^1(p) := \frac{1}{|c(d,\sqrt{E})|^2}(\Phi\sigma_1)(p), p \in B_{2\sqrt{E}}$
// $c(d,\sqrt{E})$ def. in (2.2a), Fourier transform $\mathcal{F}$ in (1.1) and $\Phi : \mathcal{M}' \to B_{2\sqrt{E}}$ in (2.10)
$u_E^1 := \texttt{reco}(Q_E^1, w, E, D, \nu_1, \tau_1)$
for *j = 1..J-1* **do**
  Compute scattering amplitude $f_{1,E}^j$ for potential $u_E^j + w$
  $Q_E^{j+1}(p) := \frac{1}{|c(d,\sqrt{E})|^2}(\Phi\sigma_1)(p) + |(\mathcal{F}(u_E^j + w))(p)|^2 - (\Phi|f_{1,E}^j|^2)(p), \quad p \in B_{2\sqrt{E}}$
  $u_E^{j+1} = \texttt{reco}(Q_E^{j+1}, w, E, D, \nu_{j+1}, \tau_{j+1})$
end

Algorithm 2(B): function $u_E^J = \texttt{reco2B}(\sigma, \sigma_1, w, E, \{\nu_1..\nu_J\}, \{\tau_1..\tau_J\}, D)$
// iterative reconstruction algorithm for Problem 2(B) with $n = 1$

Input:
$\sigma \approx \sigma[v]$: measured scattering cross section for v on $\mathcal{M}'$
$\sigma_1 \approx \sigma[v+w]$: measured scattering cross section for $v+w$ on $\mathcal{M}'$
w, E, ν_j, τ_j, and D as in Algorithm 2(A)

Output:
u_E^J: approximate reconstruction of v

$Q_E^1(p) := \frac{1}{|c(d,\sqrt{E})|^2}((\Phi\sigma_1)(p) - (\Phi\sigma)(p)), \quad p \in B_{2\nu_1\sqrt{E}}$
// $c(d,\sqrt{E})$ def. in (2.2a), Fourier transform $\mathcal{F}$ in (1.1) and $\Phi : \mathcal{M}' \to B_{2\sqrt{E}}$ in (2.10)
$u_E^1 := \texttt{reco}(Q_E^1, w, E, D, \nu_1, \tau_1)$
for *j = 1..J-1* **do**
  Compute scattering amplitudes f_E^j and $f_{1,E}^j$ for potentials u_E^j and $u_E^j + w$
  $\Sigma^j := \frac{1}{|c(d,\sqrt{E})|^2}\Phi\sigma + |\mathcal{F}u_E^j|^2 - \Phi|f_E^j|^2$
  $\Sigma_1^j := \frac{1}{|c(d,\sqrt{E})|^2}\Phi\sigma_1 + |\mathcal{F}(u_E^j + w)|^2 - \Phi|f_{1,E}^j|^2$
  $Q_E^{j+1}(p) := \Sigma_1^j(p) - \Sigma^j(p), \quad p \in B_{2\sqrt{E}}$
  $u_E^{j+1} = \texttt{reco}(Q_E^{j+1}, w, E, D, \nu_{j+1}, \tau_{j+1})$
end

In the iterative step in Algorithm 2(A) we use Lemma 3.6 with $v + w_1$ in place of v, and in Algorithm 2(B) twice with v itself and with $v + w_1$ in place of v.

We set

$$\tau_j = \tau E^{\gamma_j - 1/2} \quad \text{with} \tag{3.10a}$$

$$\alpha_j := \frac{1}{2}\frac{m-d}{\beta+d}\left(1 - \left(\frac{m-d}{m+\beta}\right)^j\right), \quad \gamma_1 := \frac{1}{2}\frac{1}{m+\beta}, \quad \gamma_{j+1} := \frac{\alpha_j + 1/2}{m+\beta}, \tag{3.10b}$$

where m, $j \in \mathbb{N}$, $m > d$, $\beta \in \mathbb{R}$, $\beta > d$. Here, m and β are the numbers in (2.37a) and (2.37d).

Theorem 3.7. *Let v, w_1 satisfy assumptions (1.3), (2.32), (2.37b), where D, Ω_1 are convex,*

and also satisfy assumptions (2.37a) and (2.37d). Let u_E^j be defined either by Algorithm 2(A) with exact data $\sigma_1 = \sigma[v + w_1]$ and $\operatorname{dist}(\Omega_1, D) > \operatorname{diam}(D)$ or by Algorithm 2(B) for exact data $\sigma = \sigma[v]$, $\sigma_1 = \sigma[v + w_1]$ and $\operatorname{dist}(\Omega_1, D) > 0$, where $\nu_j \equiv 1$ for all j, and τ_j are as in (3.10a). Then

$$\|v - u_E^j\|_{L^\infty(D)} = \mathcal{O}(E^{-\alpha_j}) \quad \text{as } E \to +\infty, \tag{3.11}$$

where α_j are defined in (3.10b), $j \in \mathbb{N}$.

Theorem 3.7 is proved in Section B of Appendix.

For α_j and γ_j in Theorem 3.7, we have that

$$\begin{aligned} &\alpha_j \to \alpha_\infty := \frac{1}{2}\frac{m-d}{\beta+d} && \text{as } j \to +\infty, \\ &\alpha_j \to \frac{j}{2} && \text{as } m \to +\infty, \\ &\alpha_\infty \to +\infty && \text{as } m \to +\infty, \end{aligned} \tag{3.12}$$

$$\gamma_j < \gamma_{j+1},\ \gamma_j \to \gamma_\infty := \frac{1}{2}\frac{1}{\beta+d} \quad \text{as } j \to \infty. \tag{3.13}$$

Therefore, the convergence in (3.11), as $E \to +\infty$, is drastically better than in (2.38), at least, for large m and j. Besides, the convergence in (3.11), as $E \to +\infty$, is similar to the somewhat more rapid convergence in (2.29) for the phased case.

Note that the iterates u_E^j of Theorem 3.7 are simpler and more rapidly convergent theoretically than the iterates constructed in [1] for finding v from $\{\sigma[v], \sigma[v + w_1], \sigma[v + w_2]\}$ and w_1, w_2 (i.e., for Problem 2(B), $d \geq 2$, $n = 2$). However, the most essential point is that the iterates u_E^j, $j \geq 1$, of Theorem 3.7 use only the differential scattering cross section $\sigma[v + w_1]$ on Γ_E and the background scatterer w_1, when $\operatorname{dist}(D, \Omega_1) > \operatorname{diam} D$.

Remark 3.8. *Apparently, it is not difficult to show that iterates u_E^j in Theorem 3.7 depend in a Lipschitz way on errors in the phaseless data. Related analysis will be developped elsewhere. This issue is also related with approximate Lipschitz stability considered in [34] for the phased case.*

4 Numerical implementation

In the following we present numerical tests for our new theoretical results presented in Section 3.2 as well as results of [41]. We proceed from the numerical implementation developed in [1] for the case of Problem 2(B) with $d \geq 2$. For simplicity, we carry out these numerical studies for the two-dimensional case $d = 2$.

4.1 Discrete grids

We assume that v and w_1 are supported in the unit disk B_1. Let

$$\mathbb{Z}_N := \left\{-\frac{N}{2}, -\frac{N}{2}+1, ..., \frac{N}{2}-1\right\}, \ \ N \in 2\mathbb{N}. \tag{4.1}$$

We represent v and w_1 by $\underline{v}$, $\underline{w}_1$ defined on the space-variable grids

$$\mathcal{X}_N := \{x = \frac{4}{N}(n_1, n_2) : n_1, n_2 \in \mathbb{Z}_N\}, \tag{4.2}$$

where $N \in 2\mathbb{N}$, $N \geq 2\sqrt{E}/\pi$.

We consider $|f(k,l)|^2$, $|f_1(k,l)|^2$ on the grid

$$\mathcal{M}_{E,M_1,M_2} := \{(k(s), l(s,t)) : s \in \mathbb{Z}_{M_1},\, t \in \mathbb{Z}_{M_2}\}, \quad M_1,\, M_2 \in 2\mathbb{N}, \tag{4.3}$$

where

$$k(s) := \sqrt{E}\left[\cos\left(2\pi\tfrac{s}{M_1}\right), \sin\left(2\pi\tfrac{s}{M_1}\right)\right]^\top,$$
$$l(s,t) = \sqrt{E}\left[\cos\left(\tfrac{2\pi s}{M_1} + \tfrac{2\pi t}{M_2}\right), \sin\left(\tfrac{2\pi s}{M_1} + \tfrac{2\pi t}{M_2}\right)\right]^\top. \tag{4.4}$$

In view of formulas (2.17), (2.33), (2.34), (3.9) for $\widehat{v}$, $\widehat{w}_1$, this leads to the following grid in Fourier space:

$$\mathcal{P}_{E,M_1,M_2} = \{p = k - l : \ (k,l) \in \mathcal{M}_{E,M_1,M_2}\}, \ M_1, \ M_2 \in 2\mathbb{N}. \tag{4.5}$$

Note that the points of $\mathcal{P}_{E,M_1,M_2}$ are located on circles (Ewald circles) of raduis $\sqrt{E}$, that intersect at the origin; see Fig. 1.

In the Fourier domain we also consider the uniform grid:

$$\mathcal{P}_N = \{p = \frac{\pi}{2}(n_1, n_2) : \ n_1, n_2 \in \mathbb{Z}_N\}. \tag{4.6}$$

In addition to $\mathcal{P}_{E,M_1,M_2}$ and $\mathcal{P}_N$, we also consider

$$\mathcal{P}_{E,M_1,M_2,N} = \mathcal{P}_{E,M_1,M_2} \cup P_N^{\text{ext}}, \tag{4.7}$$
$$\mathcal{P}_N^{\text{ext}} = \{p \in \mathcal{P}_N : p^2 > 4E\}. \tag{4.8}$$

The number N in (4.2) and (4.6)–(4.8) is the same.

In our numerical examples we use $\mathcal{P}_{E,M_1,M_2}$, $\mathcal{P}_N$ for $M_1 = 32$, $M_2 = 256$, $N = 572$, $E = 100^2$. For this choice, we have that $|\mathcal{P}_N \cap B_{2\sqrt{E}}| = 50949$, $|\mathcal{P}_{E,M_1,M_2}| = 8192$ (where $|\cdot|$ denotes the number of elements in a set), i.e. Fourier space in $B_{2\sqrt{E}}$ is severely undersampled, in particular in the neighborhood of the circle with radius $\sqrt{E}$. The resulting numerical problems and their solution will be discussed in Subsection 4.3.

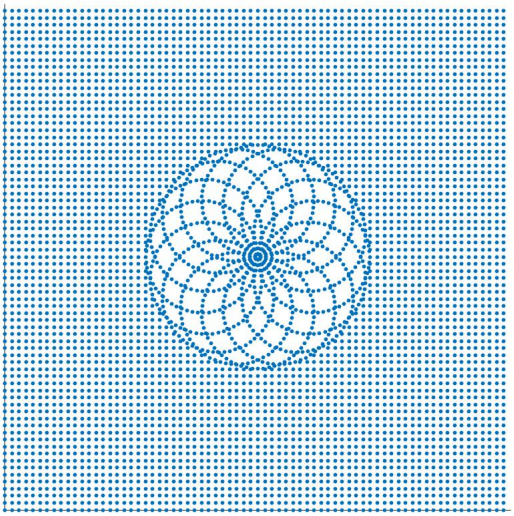

Figure 1: The grid $\mathcal{P}_{E,M_1,M_2,N}$ in Fourier space for $M_1 = 16$, $M_2 = 64$, $N = 72$, and $E = (100/8)^2$. In our numerical computations we use $M_1 = 32$, $M_2 = 256$, $N = 572$, $E = 100^2$, i.e. the same proportions. But for the later numerical parameters we have too many points to visualize.

4.2 Discrete Fourier transforms

We consider the discrete Fourier transforms F and T :

$$\underline{\widehat{u}} = F\underline{u}, \ F = [4(N\pi)^{-2}\exp(ix \cdot p)], \ x \in \mathcal{X}_N, \ p \in \mathcal{P}_N, \tag{4.9}$$
$$\underline{\widehat{u}} = T\underline{u}, \ T = [4(N\pi)^{-2}\exp(ix \cdot p)], \ x \in \mathcal{X}_N, \ p \in \mathcal{P}_{E,M_1,M_2,N}, \tag{4.10}$$

where $\underline{u}$ is a test function on $\mathcal{X}_N$ considered as a vector, and F and T are considered as matrices.

Matrix-vector products with F, its adjoint F^* as well as its inverse $F^{-1} = (\frac{\pi}{2})^4 N^2 F^*$ can be computed efficiently by the Fast Fourier Transform (FFT).

Matrix-vector products with T and T^* can also be computed efficiently by non-uniform FFT methods. We use the code NFFT 3 (see [28]) for this purpose. Computations of a left inverse of T is more difficult. One can use the conjugate gradient method applied to the normal system

$$T^*\Lambda^{1/2}T\underline{u} = T^*\Lambda^{1/2}\widehat{\underline{u}} \tag{4.11}$$

for this purpose, where Λ is a diagonal weight matrix such that $\|\Lambda^{1/2}\underline{u}\|_2^2 \approx \int |u(p)|^2 dp$; see [1, §4.1.3].

4.3 Phase retrieval with background information

In this subsection we describe our numerical implementation of Algorithm 1 for finding v from Q_E approximately given by formulas (2.39) in terms of phaseless Fourier transforms on $B_{2\sqrt{E}}$, i.e. for solving Problem 1(A) and Problem 1(B, $n = 1$). In addition, by line 1 of Alg. 1 we also define h_E which extends Q_E from $B_{2\sqrt{E}}$ to $\mathbb{R}^d$, $d = 2$. The basic point of our implementation of Algorithm 1 consists in inversion of the discrete Fourier transforms F and T. In addition, inversion of F is standard, whereas proper inversion of T includes an essential new result. Proper implementation of $(\mathcal{F}w_1(p))^{-1}\mathcal{F}q_E(p)$ in line 5 of Algorithm 1 is also essential in view of possible zeros of $\mathcal{F}w_1(p)$ (if Assumption (2.37d) is violated). Note that, for Problem 1(A) and Problem 1(B, $n = 1$) we use Algorithm 1 for cut-off parameters $\nu = \tau = 1$.

The case of data on $\mathcal{P}_N \cap B_{2\sqrt{E}}$. If in formulas (2.39) the data $Q_E(p)$ are given on $\mathcal{P}_N \cap B_{2\sqrt{E}}$, then in lines 4, 6 of Algorithm 1 we implement $\mathcal{F}^{-1}$ as F^{-1} via FFT as mentioned in Subsection 4.2.

The case of data on $\mathcal{P}_{E,M_1,M_2}$. This case is especially important for Problem 2. If in formulas (2.39) the data $Q_E(p)$ are given on $\mathcal{P}_{E,M_1,M_2}$, then line 4 of Alg. 1 we implement a left inverse of the discrete Fourier transform T using the conjugate gradient method mentioned in Subsection 4.2. However, because of the geometric constraints of our setting, in particular the condition $\operatorname{dist}(\Omega_1, D) > \operatorname{diam}(D)$, the system (4.11) is much more ill-conditioned than in [1] due to the severe undersampling of Fourier space discussed at the end of Subsection 4.1; see also Fig. 1. Therefore, the conjugate gradient method for system (4.11) does not converge properly to an approximation of $\mathcal{F}^{-1}h_E$ in line 4 of Alg. 1. To cope with this difficulty, we use a very specific property of h_E described by the formulas

$$\mathcal{F}^{-1}h(x) - W_1(x) = 0, \quad x \in \mathcal{U}^c := \mathbb{R}^d \setminus \mathcal{U}, \tag{4.12}$$

$$h(p) := \lim_{E\to+\infty} h_E(p),\ p \in \mathbb{R}^d, \tag{4.13}$$

$$\mathcal{U} := \begin{cases} (D-\Omega_1)\cup(\Omega_1-D)\cup B_{\operatorname{diam} D}, & \text{if } Q_E(p) \text{ is defined as in (2.39a)},\\ (D-\Omega_1)\cup(\Omega_1-D), & \text{if } Q_E(p) \text{ is defined as in (2.39b)}, \end{cases} \tag{4.14}$$

see formulas (47), (49), (51), (53) of [41].

It is convenient to rewrite (4.12) as

$$\mathcal{F}^{-1}\tilde{h}(x) = 0, \quad x \in \mathcal{U}^c \quad \text{with} \tag{4.15}$$

$$\tilde{h}(p) := \lim_{E\to+\infty} \tilde{h}_E(p), \quad \tilde{h}_E(p) := h_E(p) - (\mathcal{F}W_1)(p), \quad p \in \mathbb{R}^d. \tag{4.16}$$

The property (4.12), (4.15) means that $\mathcal{F}^{-1}\tilde{h}$ is identically zero on $\mathcal{U}^c$, and $\mathcal{F}^{-1}\tilde{h}_E$ is approximately zero on $\mathcal{U}^c$. Moreover, we have that:

$$\mathcal{F}^{-1}\tilde{h}_E(x) = \int_{|p|\geq 2\sqrt{E}} e^{-ipx}(|\hat{w}_1(p)|^2 - |\hat{v}(p)+\hat{w}_1(p)|^2)dp, \quad x \in \mathcal{U}^c, \tag{4.17a}$$

$$\mathcal{F}^{-1}\tilde{h}_E(x) = \int_{|p|\geq 2\sqrt{E}} e^{-ipx}(|\hat{w}_1(p)|^2 + |\hat{v}(p)|^2 - |\hat{v}(p)+\hat{w}_1(p)|^2)dp, \quad x \in \mathcal{U}^c, \tag{4.17b}$$

for the cases (A) and (B), respectively. That is, in particular, $\mathcal{F}^{-1}\tilde{h}_E$ on $\mathcal{U}^c$ depends only on a higher frequency parts of v and w_1. Formulas (4.17) follow from (4.12)–(4.16), and from the formulas

$$h_E = h - (1 - \chi_{B_{2\sqrt{E}}})|\mathcal{F}(v + w_1)|^2 + (1 - \chi_{B_{2\sqrt{E}}})|\mathcal{F}w_1|^2, \tag{4.18a}$$

$$h_E = h - (1 - \chi_{B_{2\sqrt{E}}})(|\mathcal{F}(v + w_1)|^2 - \mathcal{F}v|^2) + (1 - \chi_{B_{2\sqrt{E}}})|\mathcal{F}w_1|^2, \tag{4.18b}$$

for the cases (A) and (B), respectively, where $\chi_{B_{2\sqrt{E}}}$ is the characteristic function of $B_{2\sqrt{E}}$.

Therefore, for finding $\mathcal{F}^{-1}\tilde{h}_E$ arising in (2.39) and line 1 of Alg. 1 in place of system (4.11) we use the conjugate gradient method for the following system for $\underline{u}$ on $\mathcal{X}_N$,

$$\Pi T^* \Lambda^{1/2} T \Pi \underline{u} = \Pi T^* \Lambda^{1/2} \underline{\tilde{h}_E}, \tag{4.19}$$

where Π is the projector defined by the characteristic function $\mathcal{U}$ in (4.14), i.e.

$$\Pi \underline{u} := \chi_{\mathcal{U}} \cdot \underline{u}. \tag{4.20}$$

Note that if $\operatorname{diam}\Omega_1 \le \operatorname{diam} D$, then $\operatorname{supp} W_1 \subseteq B_{\operatorname{diam} D}$, and, therefore, (4.12), (4.15) also hold without W_1, and for finding $\mathcal{F}^{-1}h_E$ one can use (4.19) with $\underline{h}_E$ in place of $\underline{\tilde{h}_E}$.

Note also that if in Algorithm 1 the cut-off parameter $\nu \in (0, 1)$, then h_E also depends on ν, and in formulas (4.17), (4.18) the radius $2\sqrt{E}$ should be replaced by $2\nu\sqrt{E}$. The point is that such cut-off parameters ν arise in Section 4.4.

The use of initial system (4.11) without a priori information (4.12)–(4.16) results in considerable reconstruction errors of v_E in Algorithm 1 with Q_E given by (2.39), see Figs. 4, 5.

In the present work, we use 40 conjugate gradient steps for system (4.19). In contrast, even 100 conjugate gradient steps for solving system (4.11) does not lead to a proper result.

Moreover, because of accumulation of such errors, our numerical iterative reconstruction presented in Sections 3.2, 4.4 does not converge properly.

Finally, in the present work, we implement line 5 of Alg. 1 (i.e. $\widehat{v}_E \equiv (\mathcal{F}w_1)^{-1}\mathcal{F}q_E$) as

$$\frac{a}{b} \approx (1 + \varepsilon)\frac{ab^*}{bb^* + \varepsilon \max_p |b|^2} \quad \text{with} \quad a = \mathcal{F}q_E(p),\ b = \mathcal{F}w_1(p), \tag{4.21}$$

where ε is an appropriately small positive number. In our numerical examples we choose $\varepsilon = 5 \cdot 10^{-3}$. Formula (4.21) is essentially Tikhonov regularization for solving the linear equation $b\ \hat{v}_E = a$ for $\hat{v}_E \in L_2(B_r)$ where $\varepsilon \cdot \max_p |b|^2$ is the regularisation parameter. In addition, we included the factor $(1 + \varepsilon)$ in the right-hand side of (4.21) in order to have the identity $\hat{v}_{E,\varepsilon}(p) = \hat{v}_E(p)$ for $p \in \operatorname{argmax}_p |b(p)|^2$.

Note that, for example, $|\mathcal{F}w_1|^2$ has many zeros (in violation of assumption 2.37d of our theoretical analysis!) if w_1 is a multiple of the characteristic function of a box as in Fig. 2. For such cases, formulas (4.21) are very essential.

For the phase retrieval problem our numerical realisation of Algorithm 1 is summarized as Algorithm 3.

Algorithm 3: function $v = \texttt{reco\_discr}(N, M_1, M_2, Q, w, E, \nu, \tau, D, \Omega)$

Input:

$N \in 2\mathbb{N}$: The spatial grid $\mathcal{X}_N \subset [-2,2]^2$ and the Fourier grid $\mathcal{P}_N \subset [-\frac{\pi N}{4}, \frac{\pi N}{4}]^2$ have size $N \times N$; see (4.2), (4.6)

$M_1, M_2 \in \mathbb{N}$: number of incident fields and measurement points. This defines the Fourier grids $\mathcal{P}_{E,M_1,M_2}$, $\mathcal{P}_{E,M_1,M_2,N}$; see (4.5), (4.7) and Fig. 1

$Q : \mathcal{P}_{E,M_1,M_2} \to \mathbb{R}$: phaseless data given by (2.39) or (2.36) for Problems 1 and 2, rsp.

$w : \mathcal{X}_N \to \mathbb{C}$ background potential

convex $D, \Omega \subset \mathcal{X}_N$ contains support of v and w, rsp.

Output:

$v : \mathcal{X}_N \to \mathbb{C}$ approximation of unknown potential such that $\operatorname{supp} v \subseteq D$

Compute vector $\lambda : \mathcal{P}_{E,M_1,M_2,N} \to \mathbb{R}$ of areas of Voronoi cells of these points and set $\Lambda := \operatorname{diag}(\lambda)$ *// see, e.g. Fig 2 in [1]*

$\chi_D(x) := \begin{cases} 1, & x \in \mathcal{X}_N \cap D \\ 0, & x \in \mathcal{X}_N \setminus D \end{cases}$ and $\chi_{D-\Omega}(x) := \begin{cases} 1, & x \in \mathcal{X}_N \cap (D-\Omega) \\ 0, & x \in \mathcal{X}_N \setminus (D-\Omega) \end{cases}$

$\chi_{\mathcal{U}}(x) := \begin{cases} 1, & x \in \mathcal{X}_N \cap ((D-\Omega) \cup (\Omega - D) \cup B_{\operatorname{diam} D}) \\ 0, & x \in \mathcal{X}_N \setminus ((D-\Omega) \cup (\Omega - D) \cup B_{\operatorname{diam} D}) \end{cases}$

$\chi_{B_{2\tau\sqrt{E}}}(p) := \begin{cases} 1, & p \in \mathcal{P}_N \cap B_{2\tau\sqrt{E}} \\ 0, & p \in \mathcal{P}_N \setminus B_{2\tau\sqrt{E}} \end{cases}$ and $\chi_{B_{2\nu\sqrt{E}}}(p) := \begin{cases} 1, & p \in \mathcal{P}_{E,M_1,M_2} \cap B_{2\nu\sqrt{E}} \\ 0, & p \in \mathcal{P}_{E,M_1,M_2} \setminus B_{2\nu\sqrt{E}} \end{cases}$

$F := [4(N\pi)^{-2} \exp(ix \cdot p)]_{x,p}$ with $x \in \mathcal{X}_N$, $p \in \mathcal{P}_N$
// matrix-vector products with F, F^*, and F^{-1} implemented by FFT

$T := [4(N\pi)^{-2} \exp(ix \cdot p)]_{x,p}$ with $x \in \mathcal{X}_N$, $p \in \mathcal{P}_{E,M_1,M_2}$
// matrix-vector products with T and T^* implemented by non-uniform FFT

$\widehat{w} := Fw$ *// defined on $\mathcal{P}_N$*

$h = \chi_{B_{2\nu\sqrt{E}}} Q$

if $(\operatorname{diam} \Omega < \operatorname{diam} D < \operatorname{dist}(D, \Omega))$ **then**

  $rhs := \chi_{\mathcal{U}} \cdot (T^* \Lambda^{1/2} h)$

else

  $W := F^{-1}(|\widehat{w}|^2)$

  $rhs := \chi_{\mathcal{U}} \cdot T^* \Lambda^{1/2} (h - TW)$

end

Solve $\chi_{\mathcal{U}} \cdot T^* \Lambda^{1/2} T (\chi_{\mathcal{U}} \cdot q_{\text{in}}) = rhs$ for $q_{\text{in}} : \mathcal{X}_N \to \mathbb{C}$ by CG method

$q := \chi_{D-\Omega} \cdot (q_{\text{in}} + F^{-1}((1 - \chi_{B_{2\nu\sqrt{E}}}) \cdot |\widehat{w}|^2))$

$\widehat{v} := (1+\varepsilon) \chi_{B_{2\tau\sqrt{E}}} \frac{Fq \cdot \overline{\widehat{w}}}{\widehat{w} \cdot \overline{\widehat{w}} + \varepsilon \max |\widehat{w}|^2}$ with $\varepsilon := 0.005$

$v := \chi_D \cdot F^{-1}(\widehat{v})$

4.4 Phaseless inverse scattering with background information

Our numerical reconstructions are based on Algorithms 1, 2(A) and 2(B), more precisely, on discrete versions of these algorithms. Recall that in the case of Problem 2, Algorithm 1 is used to provide the first approximation and its iterative improvements in Algorithms 2(A) and 2(B). A discrete version of Algorithm 1 is given as Algorithm 3. Algorithms 2(A) and 2(B) have straightforward analogues in the discrete setting, replacing Algorithm 1 by its discrete analog, Algorithm 3.

In addition, there are the following essential points:

(i) In the numerical implementations of the present work, we fix in advance the total number J of the iterates u_E^j, $j = 1, ..., J$, where $J = 1$, $J = 6$, $J = 10$ in our examples. In addition,

our choice of the cut-off parameters ν_j, τ_j in Algorithms 2(A), 2(B) is as follows:

$$\nu_j = 0.5 + 0.5\,\frac{j-1}{J}, \quad \tau_j = 1, \;\; j = 1, ..., J. \tag{4.22}$$

Note that this choice of cut-off parameters ν, τ differs from the choice of these cut-off parameters in Theorem 3.7. The reason is that the cut-off parameters given by (4.22) yield better numerical results.

(ii) For normalized measured data $\sigma[v_1]^{\rm meas}(k,l)$, where $k \in \{k_1, ..., k_{M_1}\}$, $l \in \{l_1, ..., l_{M_2}\}$, we use the Poisson noise model in a similar way as in [1]. In this framework the noise level is characterized by the number N_p of measured particles. As mentioned in introduction, $\sigma[v_1](k,l)$ describes the probability density of scattering of particles with initial impulse k into direction $l/|l| \neq k/|k|$. We assume that for each incident impulse k_i the exposure time $t(k_i)$ is chosen such that the same expected number of particles N_p/M_1 is recorded in the sum over all l_j. Thus, our simulated normalized measured noisy data $\sigma[v_1]^{\rm meas}(k,l)$ were generated from exact data $\sigma[v_1](k,l)$ via the formulas

$$\sigma[v_1]^{\rm meas}(k_i,l_j) \sim \frac{1}{t(k_i)}\,{\rm Pois}(t(k_i)\sigma[v_1](k_i,l_j)),\; t(k_i) = \frac{N_p}{M_1\sigma[v_1](k_i)},\; \sigma[v_1](k_i) = \sum_{j=1}^{M_2}\sigma[v_1](k_i,l_j), \tag{4.23}$$

where $i = 1, ..., M_1, \;\; j = 1, ..., M_2$.

(iii) The approximation u_E^J mentioned above does not converge to v at fixed E even when J increases; see, in particular, Theorem 3.7. Therefore, we improve u_E^J using the Newton-CG method (see [19]) in a similar way with [1].
In the present work we use Newton-CG for minimizing the following quadratic approximation of the negative Poisson log-likelihood (Kullback-Leibler divergence):

$$\Delta(\sigma[v_1]^{\rm comp}, \sigma[v_1]^{\rm meas}) = \sum_{(k,l)\in\mathcal{M}_{E,M_1,M_2}} \frac{|\sigma[v_1]^{\rm comp}(k,l) - \sigma[v_1]^{\rm meas}(k,l)|^2}{\max(\varepsilon, \sigma[v_1]^{\rm meas}(k,l))}, \tag{4.24}$$

$$\varepsilon = \frac{1}{1000}\max_{(k,l)}\sigma[v_1]^{\rm meas}(k,l),$$

among all $v \in H^1$ supported in D, where $\sigma[v_1]^{\rm meas}$ is our normalized measured monochromatic phaseless scattering data defined according to (4.23), $\sigma[v_1]^{\rm comp}$ denotes the monochromatic phaseless scattering data (differential scattering cross section) computed for $v_1 = v + w$, and D is chosen as small as possible using a priori information. As initial approximation for v, one can use u_E^J mentioned above.

5 Numerical examples

5.1 Test potentials

Throughout this section we use the values of energy E and discretization parameters M_1, M_2, and N given is Subsection 4.1; see also Fig. 1. The forward problems are solved using a periodized version of the Lippmann-Schwinger equation (2.1) as proposed in [50]. Noisy Poisson distributed synthetic data $\sigma[v_1]^{\rm meas}$ on $\mathcal{M}_{E,M_1,M_2}$ are generated with an expected total number of $N_p = 3\cdot 10^7$ counts.

We consider reconstructions of two potentials v shown in Fig. 2, where v is smooth for case (a), and v is non-smooth for case (b). For Problem 2(B) with $n = 2$ or $n = 3$, similar potentials v with different scaling were used in [1]. Fig. 2 shows $v_1 = v + w$ on $\mathcal{X}_N \cap [-1,1]^2$, where $N = 572$. This w is a multiple of the characteristic function of a square and will be also denoted as $w_{\rm box}$.

We also define

$$v_E^{\rm filt} = F^{-1}(\chi_{B_{2\sqrt{E}}} \cdot F\underline{v}), \tag{5.1}$$

where $\underline{v}$ is our potential v on $\mathcal{X}_N$, F is the discrete Fourier transform defined in (4.9), $\chi_{B_{2\sqrt{E}}}$ is the characteristic function of $B_{2\sqrt{E}}$. For the potentials v shown in Fig. 2(a, b) their filtered versions $v_E^{\rm filt}$ are shown in Fig. 3(a, b). The point is that in the present work we do not try to reconstruct v much better than $v_E^{\rm filt}$ proceeding from the scattering data $\sigma[v_1]^{\rm meas}$ at fixed energy E.

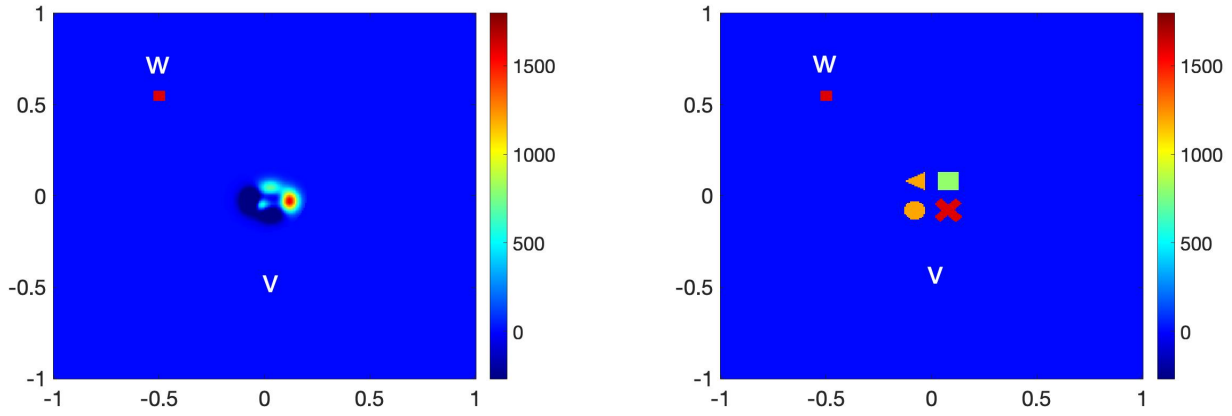

(a) (b)

Figure 2: Test examples for the unknown potential v and the known background potential w. (a) Smooth v. (b) Non-smooth v.

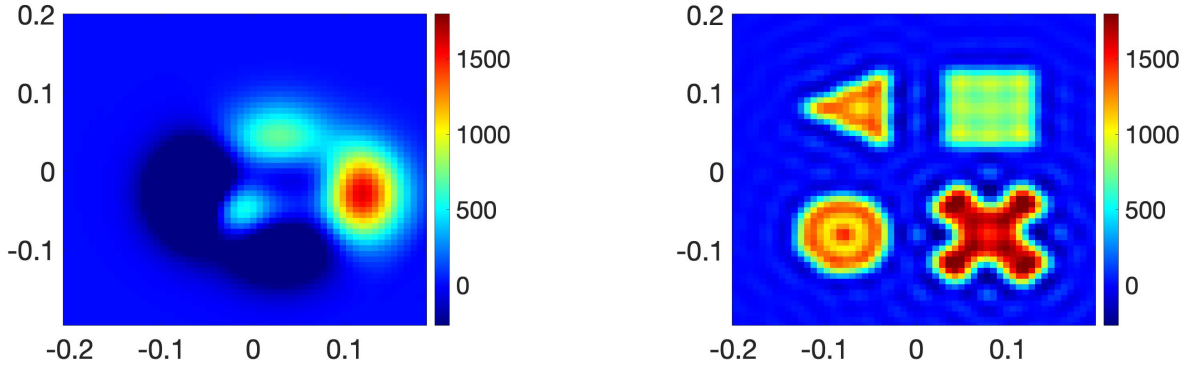

(a) (b)

Figure 3: Filtered versions $v_E^{\rm filt}$ of the test potentials v in Fig. 2 corresponding to ideal reconstructions within the classical diffraction limit for the chosen energy $E = 100$ (see (5.1)). (a) Smooth v : $\mathfrak{E}(v_E^{\rm filt}, v) = 0.0077$. (b) Non-smooth v : $\mathfrak{E}(v_E^{\rm filt}, v) = 0.2808$.

To measure the quality of numerical reconstructions, we use the relative error

$$\mathfrak{E}(u, u_0) = \frac{\|u - u_0\|_{\ell^2(G)}}{\|u_0\|_{\ell^2(G)}}, \tag{5.2}$$

where u, u_0 are functions on some grid G.

5.2 Reconstruction results for Problem 1(A)

As approximate solutions of Problem 1(A) or Problem 2(A), we consider the result v_E of Algorithm 1 with input data Q_E defined by formula (2.39a) or (2.36a), respectively. First, Fig. 4 (a, b)

illustrate our reconstructions v_E from $|\mathcal{F}(v+w)|^2$ given on the uniform grid $\mathcal{P}_N \cap B_{2\sqrt{E}}$ as described in Subsection 4.3. Then, Fig. 5 (a0, b0) illustrate our reconstructions v_E of v from $|\mathcal{F}(v+w)|^2$ on $\mathcal{P}_{E,M_1,M_2}$, where we use system (4.11) (with 40 conjugate gradient steps) for inverting the discrete Fourier transform T. Finally, Fig. 5 (a, b) illustrate our reconstructions v_E of v from $|\mathcal{F}(v+w)|^2$ on $\mathcal{P}_{E,M_1,M_2}$, where we use modified system (4.19) (with 40 conjugate gradient steps) in place of (4.11). The point is that system (4.19) leads to much better result. More precisely, these figures show our reconstructions v_E of smooth and non-smooth v shown on Fig. 2(a, b) from discrete phaseless Fourier data without Poisson noise.

One can see that reconstructions v_E shown at Fig. 4 and Fig. 5(a, b) are rather good, especially for the case of smooth v, when $\mathcal{F}v$ is rather small on $\mathbb{R}^2 \setminus B_{2\sqrt{E}}$, and also for the case of non-smooth v, in comparison with $v_E^{\rm filt}$.

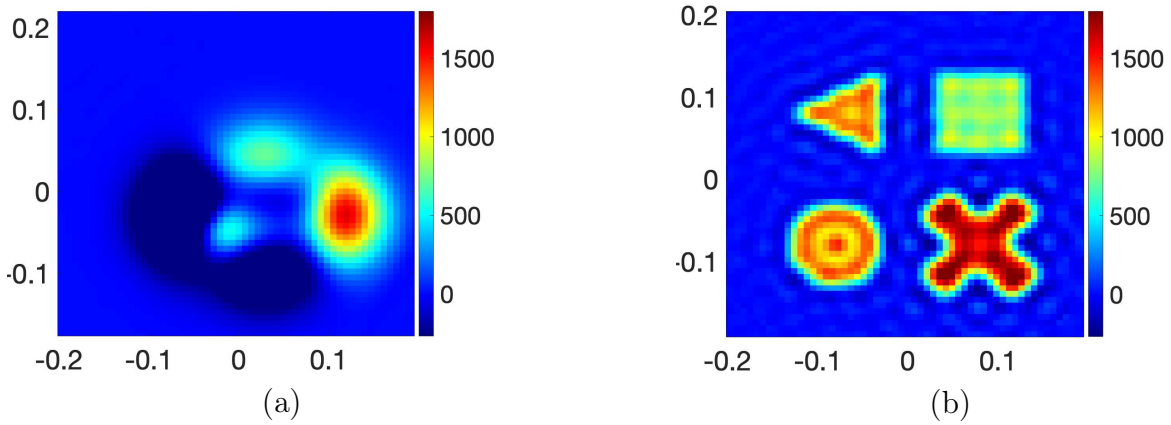

Figure 4: Reconstructions v_E from $|\mathcal{F}(v+w)|^2$ on $\mathcal{P}_N \cap B_{2\sqrt{E}}$.
(a) Smooth v : $\mathfrak{E}(v_E, \underline{v}) = 0.005$, $\mathfrak{E}(v_E, v_E^{\rm filt}) = 0.001$. (b) Non-smooth v : $\mathfrak{E}(v_E, \underline{v}) = 0.2816$, $\mathfrak{E}(v_E, v_E^{\rm filt}) = 0.0292$.

5.3 Basic reconstruction results for Problem 2(A)

In this subsection we present our reconstructions for Problem 2(A) with the test potentials v and w described in Subsection 5.1 and shown in Fig. 2. In particular, Fig. 6 and Fig. 7 illustrate our reconstructions of v from $\sigma[v_1]^{\rm meas}$ on $\mathcal{M}_{E,M_1,M_2}$ with known background w. More precisely, these figures show our reconstructions u_E^J, u_E^{J+K} of smooth and non-smooth potentials v shown on Fig. 2(a, b). Here, u_E^J are as described in Section 4.4, and u_E^{J+K} denotes u_E^J improved by K iterations of Newton-CG method. In addition: $J = 1$ for Fig. 6 (a, d), Fig. 7 (a, d), $J = 6$ for Fig. 6 (b, e), $J = 10$ for Fig. 7 (b, e), $J = 6$, $K = 5$ for Fig. 6 (c, f), $J = 10$, $K = 5$ for Fig. 7 (c, f). In addition, Fig. 6 and Fig. 7 also show the relative reconstruction errors with respect to both v and $v_E^{\rm filt}$.

One can see that already reconstruction u_E^1 going back to [41] and illustrated in Fig. 6 (a, d) with $\mathfrak{E}(u_E^1, \underline{v}) = 0.4112$ and in Fig. 7 (a, d) with $\mathfrak{E}(u_E^1, \underline{v}) = 0.5140$ is of interest in spite of considerable errors in real and imaginary parts $\operatorname{Re} u_E^1$ and $\operatorname{Im} u_E^1$ of u_E^1. These considerable errors in u_E^1 arise as a consequence of large strength of v, yielding the Born approximation unsatisfactory. Next, one can see that reconstruction u_E^J developed in the present work for $J > 1$ (for the case beyond the Born approximation) and illustrated in Fig. 6 (b, e) and in Fig. 7 (b, e) is considerably more precise than u_E^1 for reasonably large E and J. Finally, similar to [1], one can see that u_E^{J+K} improves u_E^J, under the condition that u_E^J is close to v.

The visual quality of our phaseless inverse scattering reconstructions u_E^J, u_E^{J+K} shown at Fig. 6 and Fig. 7 (for $J > 1$) turns out to be more or less comparable with our phaseless Fourier reconstructions v_E shown at Fig. 5(a, b) and even at Fig. 4. In addition, the errors $\mathfrak{E}(v_E, \underline{v})$ shown at Fig. 7, for $v_E = u_E^{10}$, u_E^{10+5}, are also comparable with the error $\mathfrak{E}(v_E, \underline{v})$ shown at Fig. 5(b). Besides, the errors $\mathfrak{E}(v_E, \underline{v})$ shown at Fig. 6, for $v_E = u_E^6$, u_E^{6+5}, reduce considerably for $v_E = u_E^{6+K}$

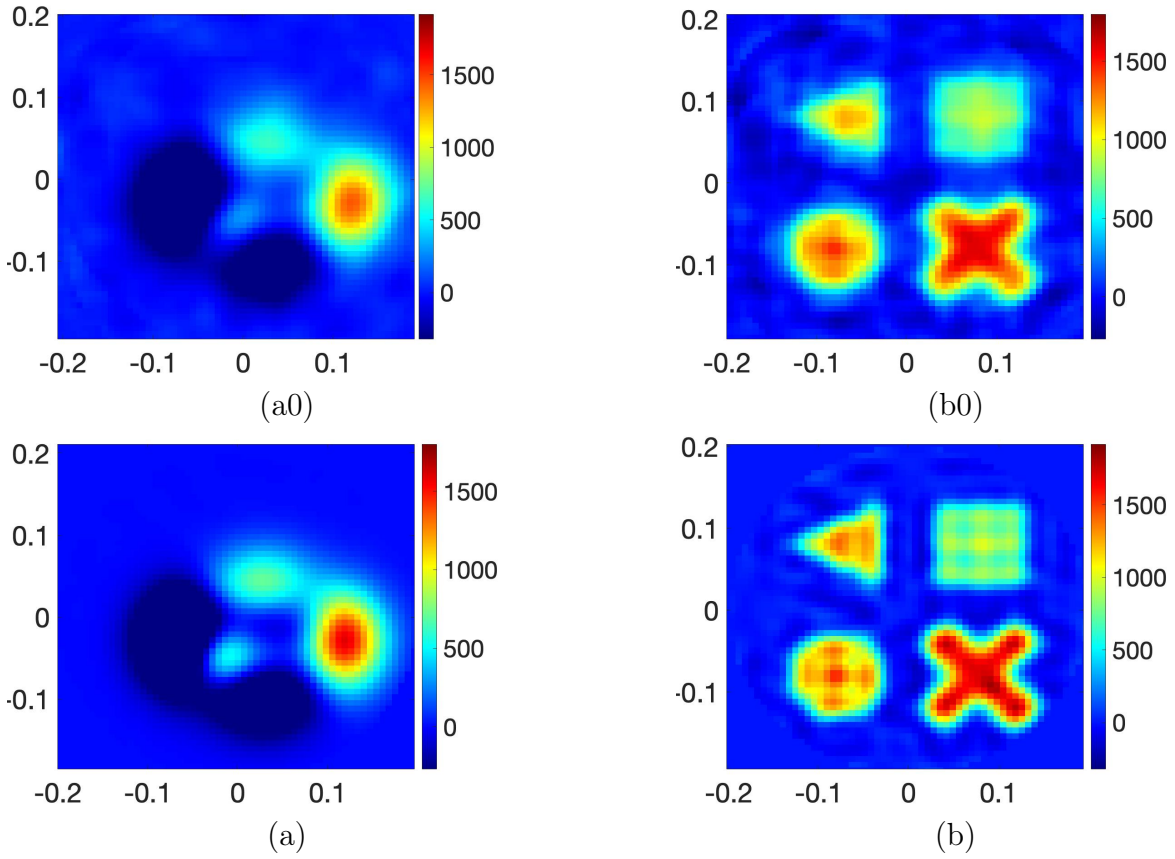

Figure 5: Reconstructions v_E from $|\mathcal{F}(v+w)|^2$ on $\mathcal{P}_{E,M_1,M_2}$.
(a0, b0): inverting T via (4.11) (old method). (a, b): inverting T using (4.19) (new method).
(a0) Smooth v : $\mathfrak{E}(v_E, \underline{v}) = 0.1417$, $\mathfrak{E}(v_E, v_E^{\text{filt}}) = 0.1416$. (b0) Non-smooth v : $\mathfrak{E}(v_E, \underline{v}) = 0.4017$, $\mathfrak{E}(v_E, v_E^{\text{filt}}) = 0.3002$. (a) Smooth v : $\mathfrak{E}(v_E, \underline{v}) = 0.01434$, $\mathfrak{E}(v_E, v_E^{\text{filt}}) = 0.01376$. (b) Non-smooth v : $\mathfrak{E}(v_E, \underline{v}) = 0.3223$, $\mathfrak{E}(v_E, v_E^{\text{filt}}) = 0.1632$.

for large K, see Fig. 8(c). For proper comparisons, recall also that the phaseless scattering data $\sigma[v_1]^{meas}$ used for the reconstructions of Fig. 6 and Fig. 7 are with Poisson noise, whereas there is no Poisson noise in the phaseless Fourier transforms used for the reconstructions of Fig. 4 and 5. In addition, the reconstructions of Fig. 4 do not have non-uniform grid difficulties.

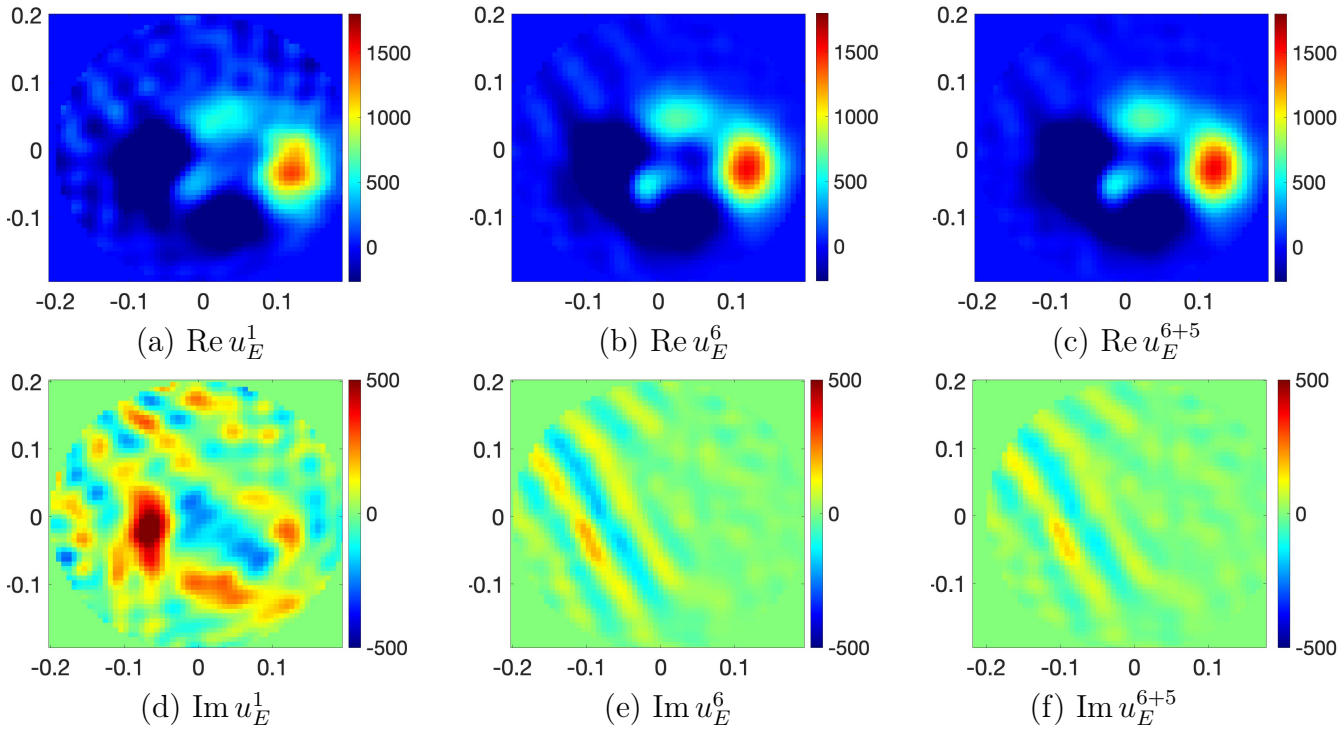

(a) $\mathrm{Re}\, u_E^1$ (b) $\mathrm{Re}\, u_E^6$ (c) $\mathrm{Re}\, u_E^{6+5}$

(d) $\mathrm{Im}\, u_E^1$ (e) $\mathrm{Im}\, u_E^6$ (f) $\mathrm{Im}\, u_E^{6+5}$

Figure 6: Reconstructions u_E^J, u_E^{J+K} of smooth v (see Fig. 2) in Problem 2(A). Top row: Real parts. Bottom row: Imaginary parts. Relative errors on $\mathcal{X}_N \cap D$: $\mathfrak{E}(u_E^1, \underline{v}) = 0.4096$, $\mathfrak{E}(u_E^1, v_E^{\mathrm{filt}}) = 0.4096$; $\mathfrak{E}(u_E^6, \underline{v}) = 0.1722$, $\mathfrak{E}(u_E^6, v_E^{\mathrm{filt}}) = 0.1722$; $\mathfrak{E}(u_E^{6+5}, \underline{v}) = 0.1257$, $\mathfrak{E}(u_E^{6+5}, v_E^{\mathrm{filt}}) = 0.1256$.

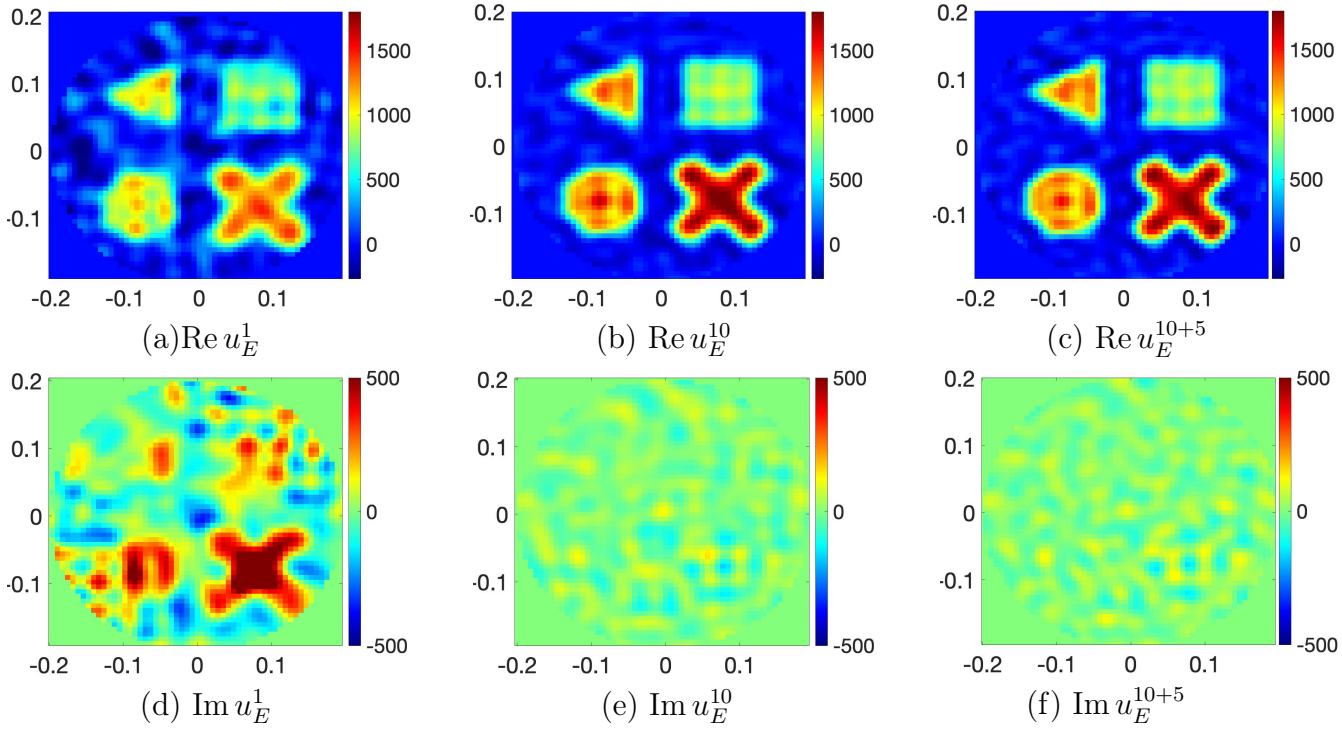

(a)$\mathrm{Re}\, u_E^1$ (b) $\mathrm{Re}\, u_E^{10}$ (c) $\mathrm{Re}\, u_E^{10+5}$

(d) $\mathrm{Im}\, u_E^1$ (e) $\mathrm{Im}\, u_E^{10}$ (f) $\mathrm{Im}\, u_E^{10+5}$

Figure 7: Reconstructions u_E^J, u_E^{J+K} of non-smooth v (see Fig. 2) in Problem 2(B) with $n = 1$. Top row: Real parts. Bottom row: Imaginary parts. Relative errors on $\mathcal{X}_N \cap D$: $\mathfrak{E}(u_E^1, \underline{v}) = 0.5140$, $\mathfrak{E}(u_E^1, v_E^{\mathrm{filt}}) = 0.4466$; $\mathfrak{E}(u_E^{10}, \underline{v}) = 0.3396$, $\mathfrak{E}(u_E^{10}, v_E^{\mathrm{filt}}) = 0.1873$; $\mathfrak{E}(u_E^{10+5}, \underline{v}) = 0.3196$, $\mathfrak{E}(u_E^{10+5}, v_E^{\mathrm{filt}}) = 0.1486$.

Next, for our smooth and non-smooth v, Fig. 8 shows L_2 discrepancies $\mathfrak{E}(j) = \mathfrak{E}(\sigma[u_E^j + w_1]^{\mathrm{comp}}, \sigma[v_1]^{\mathrm{meas}})$ Poisson discrepancies $\Delta(j) = \Delta(\sigma[u_E^j + w_1]^{\mathrm{comp}}, \sigma[v_1]^{\mathrm{meas}})$ on $\mathcal{M}_{E,M_1,M_2}$, and

relative errors $\mathfrak{E}(u_E^j, v)$ on $\mathcal{X}_N \cap D$ for the iterates u_E^j, where

$$u_E^0 \equiv 0, \tag{5.3a}$$

$$u_E^j,\ j = 1, ..., J, \text{are defined as described in item (i) of Subsection 4.4,} \tag{5.3b}$$

$$u_E^{J+k} \text{ denotes } u_E^J \text{ improved by } k \text{ iterations of Newton-CG method.} \tag{5.3c}$$

Note that $J > 0$ for the plots 'Our + NCG', and $J = 0$ for the plots 'NCG method'.

These figures also show L_2 discrepancy $\mathfrak{E}_{\text{noise}}$ and Poisson discrepancy Δ_{noise} defined by

$$\mathfrak{E}_{\text{noise}} = \mathfrak{E}(\sigma[v_1], \sigma[v_1]^{\text{meas}}), \tag{5.4}$$

$$\Delta_{\text{noise}} = \Delta(\sigma[v_1], \sigma[v_1]^{\text{meas}}), \tag{5.5}$$

or, in other words, the noise level in $\sigma[v_1]^{\text{meas}}$ in different senses. For the plots 'Our + NCG', one can see that $\mathfrak{E}(J)$ and $\Delta(J)$ are much smaller than $\mathfrak{E}(1)$ and $\Delta(1)$, respectively. However, $\mathfrak{E}(j)$ and $\Delta(j)$ are not monotonically decreasing in $j = 1, ..., J$. The reason is that the proposed iterative algorithm does not minimize the aforementioned discrepancies directly; this algorithm is based on a different principle. In addition, one can see that $\mathfrak{E}(j)$ and $\Delta(j)$ are monotonically decreasing for $j \geq J$. The reason is that the additional Newton-CG method directly minimizes $\Delta(j)$.

One can see that:

- $\mathfrak{E}(j)$ and $\Delta(j)$, for large j, are very close to the noise levels $\mathfrak{E}_{\text{noise}}$ and Δ_{noise} for smooth v;
- $\mathfrak{E}(j)$ and $\Delta(j)$, for large j, are not yet very close to the noise levels $\mathfrak{E}_{\text{noise}}$ and Δ_{noise} for non-smooth v.

The reason is that our monochromatic iterative algorithm (including additional NCG iterations) reconstruct $\hat{v}(p)$ for $|p| \leq 2\sqrt{E}$ much better than for $|p| \geq 2\sqrt{E}$.

For our examples we have that our reconstructions u_E^J give good results in configuration space (i.e., on $\mathcal{X}_N \cap D$) much faster than the Newton-CG iterates u_E^{0+k}, which start from the zero approximation, and even than u_E^{1+k}, which start from our reconstruction in the Born approximation, i.e., from u_E^J, $J = 1$. In particular, in our examples much faster means that our reconstruction u_E^J, $J = 1$, is similar to u_E^{0+18}, in the configuration space for non-smooth v, and u_E^J, $J = 1$, is similar to u_E^{0+8}, in the configuration space for smooth v. For more comparisons, see also Fig. 8.

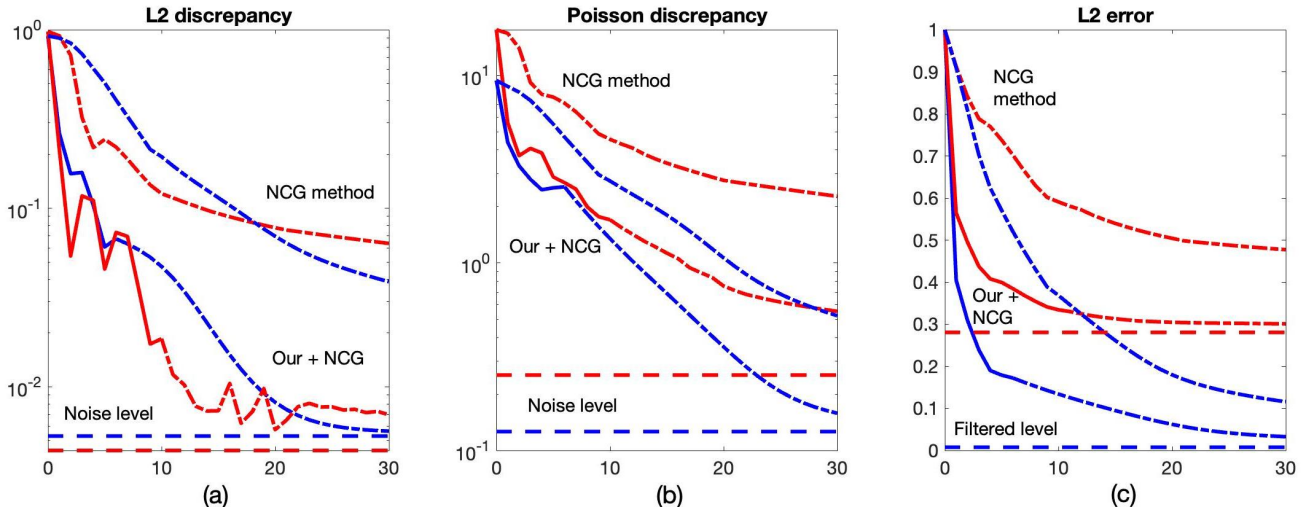

Figure 8: L_2 discrepancy $\mathfrak{E}(\sigma[u_E^j + w_1]^{\text{comp}}, \sigma[v_1]^{\text{meas}})$, Poisson discrepancy $\Delta(\sigma[u_E^j + w_1]^{\text{comp}}, \sigma[v_1]^{\text{meas}})$ and relative errors $\mathfrak{E}(u_E^j, \underline{v}, D)$ as a function of j, in comparison with $\mathfrak{E}_{\text{noise}}$ and Δ_{noise} (horizontal lines). Solid lines indicate our iterations for $j = 1, ..., J$, dashed line indicate Newton-CG (NCG) iterations. Blue: smooth v. Red: non-smooth v. For the plots 'Our + NCG', the NCG iterations start with $j = J + 1 = 7$ for smooth v and $j = J + 1 = 11$ for non-smooth v. See notations (5.3).

5.4 Further reconstruction results for Problem 2(A)

Reconstruction examples presented in this subsection are as follows: reconstruction of complex v; reconstruction with background w satisfying the additional theoretical assumption (2.37d); reconstruction of real v taking into account a priori knowledge of real-valuedness; examples of v and w for which our method converges, whereas NCG method diverges. The expected number of particles $N_p = 3 \cdot 10^7$ characterizing Poisson noise is as in Subsection 5.3.

Fig. 9 illustrates our reconstructions u_E^J, for $J = 1$, $J = 6$, and u_E^{J+K}, for $J = 6$, $K = 5$, of complex-valued potential. Here, $\operatorname{Re} v$ is two times smaller than in v in Fig. 2(a), $\operatorname{Im} v \le 0$, and $|\operatorname{Im} v|$ is four times smaller than v in Fig. 2(b), and background w is the same as in Fig. 2.

It is remarkable that our method reconstructs two real-valued functions $\operatorname{Re} v$ and $\operatorname{Im} v$ on $\mathcal{X}_N$ from one real-valued function $\sigma[v_1]^{meas}$ on $\mathcal{M}_{E,M_1,M_2}$ for known background w.

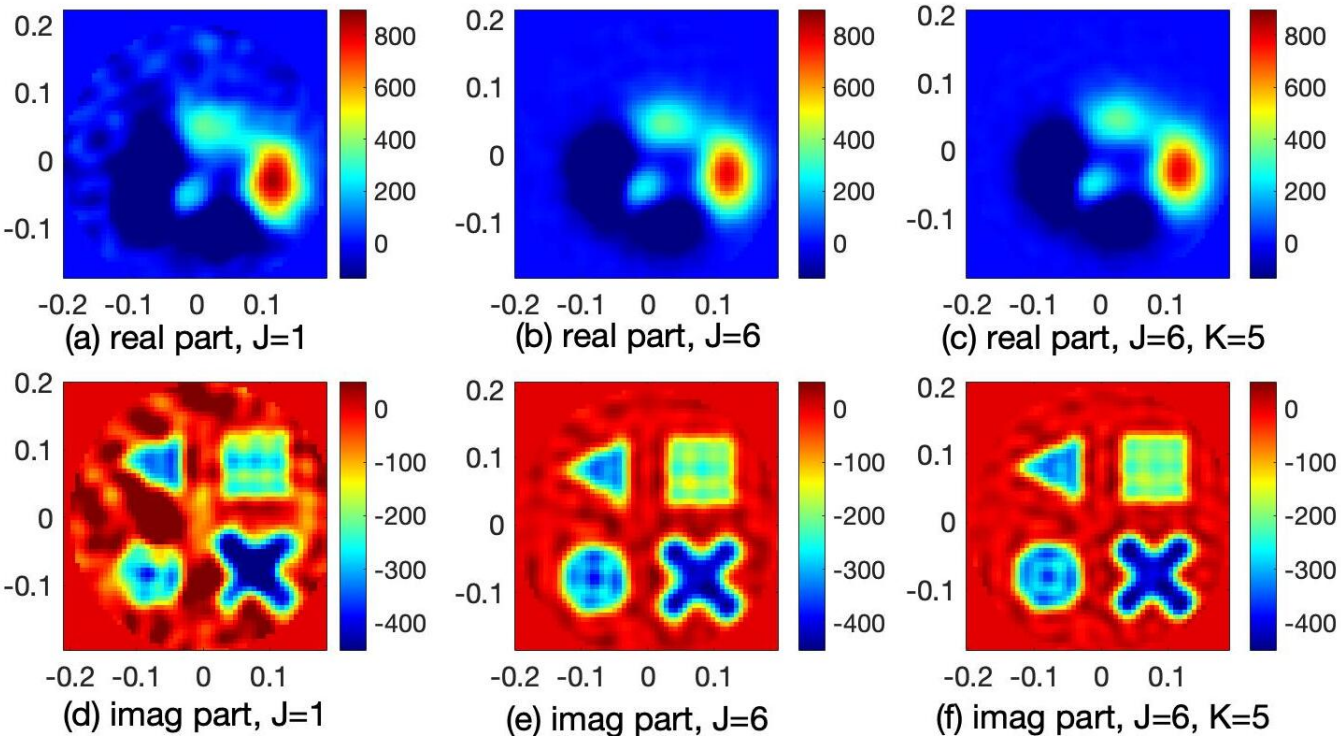

Figure 9: Reconstructions u_E^J and u_E^{J+K} of complex-valued v with smooth $\operatorname{Re} v$ and non-smooth $\operatorname{Im} v \le 0$. $\mathfrak{E}(u_E^1, v, D) = 0.3927$, $\mathfrak{E}(u_E^6, v, D) = 0.2080$, $\mathfrak{E}(u_E^{6+5}, v, D) = 0.1911$.

Next, we study our numerical reconstructions u_E^J and u_E^{J+K} for the case when w satisfies the additional theoretical assumption (2.37d). We consider w of the form

$$w = w_\Phi(x) = \lambda_1 \Phi_1(|x - x_0|/\lambda_2), \quad \lambda_1,\, \lambda_2 > 0,\, x,\, x_0 \in \mathbb{R}^2, \tag{5.6a}$$

$$\Phi_1(r) = \max(1 - r, 0)^4 (4r + 1). \tag{5.6b}$$

Here, Φ_1 is one of Wendland's radial functions. In particular, w_Φ given by (5.6) satisfies (2.37d) with $\beta = 5$, $d = 2$, and $w_\Phi \in C^2(\mathbb{R}^d)$, see [1], [51]. We chose λ_1, λ_2, x_0 in a such way that x_0 is the center of w_{box}, $2\lambda_2$ is the length of the side of $\operatorname{supp}(w_{\text{box}})$, and λ_1 is such that $\|w_\Phi\|_{L_2} = \|w_{\text{box}}\|_{L_2}$, where w_{box} is w shown in Fig. 2.

Our numerical reconstructions with background w_Φ were implemented with $\varepsilon = 0$ in (4.21), taking into account that $\widehat{w}_\Phi(p)$ is not too small on $B_{2\sqrt{E}}$. These reconstructions are more or less similar in quality to our reconstructions with background w_{box} presented in Subsection 5.3; see Table 1.

Table 1 shows relative L_2 errors $\mathfrak{E}(u, v)$ and $\mathfrak{E}(u, v_E^{\text{filt}})$ on $\mathcal{X}_N \cap D$ for different reconstructions u for smooth and non-smooth real v shown on Fig. 2, where $w = w_{\text{box}}$ shown in Fig. 2, or $w = w_\Phi$

mentioned above, and $u = u_E^J$ or $u = u_E^{J+K}$. In addition, these reconstructions u are implemented either without or with the a priori assumption that $\operatorname{Im} v \equiv 0$. These reconstructions u for $w = w_{\text{box}}$ without a priori assumption that $\operatorname{Im} v \equiv 0$ are also shown in Fig. 6, 7.

Smooth v	w_{box}	w_Φ	w_{box} + $\operatorname{Im} v = 0$	w_Φ + $\operatorname{Im} v = 0$
$J = 1$	0.4096	0.3787	0.2165	0.1851
$J = 6$	0.1722	0.2222	0.0299	0.0284
$J = 6,\ K = 5$	0.1257	0.1672	0.0153	0.0159

(a) v shown in Fig. 2(a).

Non-smooth v	w_{box}	w_Φ	w_{box} + $\operatorname{Im} v = 0$	w_Φ + $\operatorname{Im} v = 0$
$J = 1$	0.5140	0.4730	0.4249	0.3803
$J = 10$	0.3396	0.3214	0.3325	0.2849
$J = 10$, $K = 5$	0.3196	0.3009	0.3048	0.2788

(b1) v shown in Fig. 2(b).

Non-smooth v vs v_E^{filt}	w_{box}	w_Φ	w_{box} + $\operatorname{Im} v = 0$	w_Φ + $\operatorname{Im} v = 0$
$J = 1$	0.4466	0.3964	0.3299	0.2667
$J = 10$	0.1873	0.1643	0.1825	0.0527
$J = 10$, $K = 5$	0.1486	0.1196	0.1329	0.0453

(b2) v_E^{filt} shown in Fig. 3(b).

Table 1: Relative L_2 errors $\mathfrak{E}(u, v)$ and $\mathfrak{E}(u, v_E^{\text{filt}})$ on $\mathcal{X}_N \cap D$ for different reconstructions u for smooth and non-smooth real v without and with the a priori assumption that $\operatorname{Im} v \equiv 0$, where $w = w_{\text{box}}$ or $w = w_\Phi$, and $u = u_E^J$ or $u = u_E^{J+K}$. (a) $\mathfrak{E}(u, v)$; (b1) $\mathfrak{E}(u, v)$; (b2) $\mathfrak{E}(u, v_E^{\text{filt}})$.

One can see that, in our examples, the use of the a priori assumption $\operatorname{Im} v \equiv 0$ strongly reduces $\mathfrak{E}(u, v)$ for smooth v and $\mathfrak{E}(u, v_E^{\text{filt}})$ for non-smooth v with $w = w_\Phi$.

Next, it is important to note that in some cases the reconstruction based completely on the NCG iterations with the zero initialization does not converges to the correct solution, whereas our method does. In particular, we obtained such examples as follows:

(a) We take v which is 5 times smaller and w which is 100 times smaller than v, w shown in Fig. 2(a);

(b) We take v which is 10 times smaller and w which is 50 times smaller than v, w shown in Fig. 2(b).

Fig. 10 shows the L_2 discrepancy $\mathfrak{E}(\sigma[u_E^j + w_1]^{\text{comp}}, \sigma[v_1]^{\text{meas}})$ on $\mathcal{M}_{E,M_1,M_2}$ and relative error $\mathfrak{E}(u_E^j, v)$ on $\mathcal{X}_N \cap D$ as functions of j, where u_E^j are constructed via our method (solid lines) and NCG method (dash lines). Note that Fig. 10(a) shows that the L_2 discrepancy asymptotically decreases even for the pure NCG method (i.e., with zero initialization), i.e., the pure NCG method converges to some local minimum. In contrast, Fig. 10(b) shows that the pure NCG method fails to converge to the global minimum, whereas our iterations do converge properly.

Note that in this example the background potential is very small in comparison to unknown potential. Recall that for zero background Problem 1 does not have unique solution. Therefore, for relatively small potentials one can expect instability of convergence of iterative NCG method. In contrast, lines 3–6 of Alg. 3 are exact, and they are more stable for relatively small w.

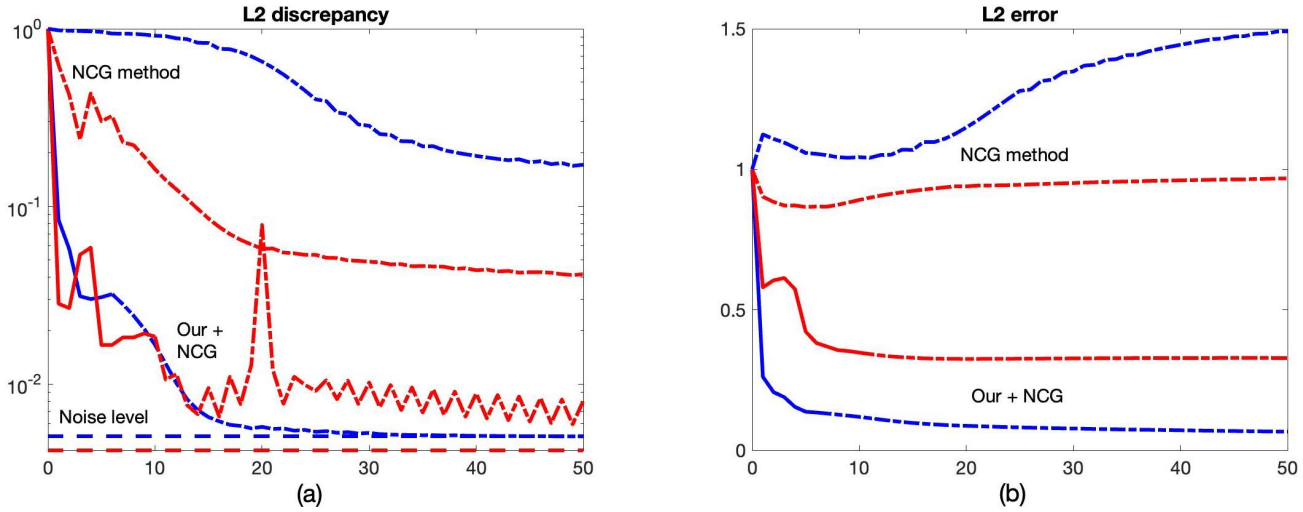

Figure 10: L_2 discrepancy $\mathfrak{E}(\sigma[u_E^j + w_1]^{\text{comp}}, \sigma[v_1]^{\text{meas}})$ and relative error $\mathfrak{E}(u_E^j, v)$ as functions of j, in comparison with $\mathfrak{E}_{\text{noise}}$ in (5.4) (horizontal lines). Solid lines indicate our iterations for $j = 1, ..., J$, dashed line indicate Newton-CG iterations. Blue: smooth v. Red: non-smooth v. For the plots 'Our + NCG', the NCG iterations start with $j = J + 1 = 7$ for smooth v and $j = J + 1 = 11$ for non-smooth v. See notations (5.3).

6 Conclusions

In the present work we present new results on phaseless monochromatic inverse scattering with only one known background scatterer.

In comparison with [1], we reduce the required amount of data by a factor three: Theoretically, [1] deals with Problem 2(B) for $d \geq 2$ and $n = 2$, that is approximately reconstructs v from the three differential scattering cross sections $\{\sigma[v], \sigma[v + w_1], \sigma[v + w_2]\}$ with known background scatterers w_1, w_2, developing methods of [2], [35], [37]. In addition, numerically, [1] deals with Problems 1(B) and 2(B) for $d = 2$ and $n = 2$ or $n = 3$. In turn, the present work deals with Problems 1(B) and 2(B) for $d = 2$ and $n = 1$ or even Problems 1(A) and 2(A) developing theoretical and numerical methods of [1], [35], [41]. In the latter case only one differential scattering cross section $\sigma[v + w_1]$ is needed.

In comparison with [41], in particular, we take into account multiple scattering in the framework of monochromatic iterative reconstruction algorithm and develop numerical implementations, using approaches of [1], [35]. Theoretically, [41] deals only with the reconstructions given by Algorithm 1 with Q_E given by (2.39) for phaseless Fourier inversion, and by formulas (2.36), (2.10) for phaseless inverse Born scattering, without numerical implementation yet. The present work strongly develops these theoretical results already by Theorem 3.2 for phaseless Fourier inversion and mainly by Theorem 3.7 for phaseless inverse non-linearised scattering. In particular, we establish rapid convergence of approximate monochromatic reconstructions v_E and u_E^j to v, as $E \to +\infty$. Moreover, in the present work we implement numerically theoretical results of [41] and of our new theoretical results in Theorem 3.2 and Theorem 3.7.

In some respects the properties of the numerical implementations of the present work are similar to those in [1]: inversion of the discrete non-uniform Fourier transform T mentioned in Section 4.2 is realised using the conjugate gradient method; iterative reconstructions use the same solver for direct scattering problems; mathematical justification of these iterations goes back to [35]; at the end the reconstruction results are improved using the Newton-CG method; the same Poisson model for noisy data is used.

The main differences are as follows: theoretical reconstruction formulas are essentially different already in the Born approximation and then for iterations; required grid sizes are significantly larger in view of conditions like $\text{dist}(D, \Omega_1) > \text{diam}\, D$ required in [41] and the present work (see

Section 2.3); the initial CG approach for inversion of T was not working properly for reconstructions of the present work and we modified it taking into account a priori information given by theoretical formulas (4.12)–(4.14) recalled in Section 4.3; less measurements and a lower total number of 'Poisson count's, and less direct problem solutions are needed by the numerical methods of the present work.

Natural further research includes study of applicability limits of numerical implementations with respect to different parameters of the algorithm, extension of the numerical implementations to the three-dimensional case, and reconstructions from real data. The experimental scheme could be similar to that in [43].

Acknowledgements

We thank A.D. Agaltsov and G.V. Sabinin for valuable discussions in connection with numerical codes and A.S. Shurup for valuable advice in connection with some issues of numerical implementation.

T. Hohage acknowledges financial support by the Deutsche Forschungsgemeinschaft (DFG, German Research Foundation) – Project-ID 432680300 – SFB 1456.

V. N. Sivkin is supported by RSF, grant № 20-11-20261.

V. N. Sivkin is fellow of the Foundation for the Advancement of Theoretical Physics and Mathematics "BASIS".

Appendix A Proof of Lemma 3.6.

To prove Lemma 3.6 we use, in particular, Lemma 2.1 and the following additional lemma.

Lemma A.1. *Under the assumptions of Lemma 2.1, the following estimates hold:*

$$|f(k,l)| \le \frac{3}{2}(2\pi)^{-d} N c_1^2(d,s), \tag{A.1}$$

$$|f(k,l) - f_{\text{appr}}(k,l)| \le (2\pi)^{-d} c_4(s,D) b E^{-\alpha}, \tag{A.2}$$

$$c_4(s,D) = \left(3c_1^2(d,s)c_5(D,s) + \mu(D)\right)$$

where $(k,l) \in \mathcal{M}_E$, $E^{1/2} \ge \rho_1(d,s,N)$, c_1 *is given by (2.19),* $c_5(D,s) = \max_D(1+|x|^2)^{s/2}$.

Proof. We have that

$$|f(k,l)| \le |f(k,l) - \widehat{v}(k-l)| + |\widehat{v}(k-l)|. \tag{A.3}$$

Using (1.1), (2.5), (2.18)–(2.20), (A.3) we obtain that

$$\begin{aligned} &|f(k,l)| \le 2^{-1}(2\pi)^{-d} c_1^2(d,s)\|v\|_s + (2\pi)^{-d} c_1^2(d,s)\|v\|_s = \frac{3}{2}(2\pi)^{-d} c_1^2(d,s)\|v\|_s, \\ &(k,l) \in \mathcal{M}_E,\ E^{1/2} \ge \rho_1(d,s,N). \end{aligned} \tag{A.4}$$

Thus, estimate (A.1) is proved.

Next, we have that

$$|f(k,l) - f_{\text{appr}}(k,l)| \le |\delta f(k,l) - \delta f_{\text{appr}}(k,l)| + |\widehat{v}(k-l) - \widehat{v}_{\text{appr}}(k-l,E)|, \tag{A.5}$$

where

$$f(k,l) = \widehat{v}(k-l) + \delta f(k,l), \tag{A.6}$$

$$f_{\text{appr}}(k,l) = \widehat{v}_{\text{appr}}(k-l,E) + \delta f_{\text{appr}}(k,l). \tag{A.7}$$

Due to formula (4.11) of [35], we have that

$$|\delta f(k,l) - \delta f_{\rm appr}(k,l)| \le 6(2\pi)^{-d} a_0(d,s/2) c_1^2(d,s) c_5(D,s) \|v\|_s b E^{-\alpha-1/2}, \\ (k,l) \in \mathcal{M}_E,\ E^{1/2} \ge \rho_1(d,s,N). \tag{A.8}$$

Using (1.1), (2.5), (2.19)–(2.22), (A.5), (A.8), we obtain that

$$\begin{aligned} |f(k,l) - f_{\rm appr}(k,l)| &\le 3(2\pi)^{-d} c_1^2(d,s) c_5(D,s) b E^{-\alpha} + (2\pi)^{-d} \mu(D) b E^{-\alpha} \\ &= (2\pi)^{-d} \left(3 c_1^2(d,s) c_5(D,s) + \mu(D)\right) b E^{-\alpha}, \\ &\text{for } (k,l) \in \mathcal{M}_E, \quad E^{1/2} \ge \rho_1(d,s,N). \end{aligned} \tag{A.9}$$

Thus, estimate (A.2) is proved. □

We set:

$$\Delta_1 = f - \widehat{v} - f_{\rm appr} + \widehat{v}_{\rm appr}, \tag{A.10}$$

$$\Delta_2 = f - f_{\rm appr}. \tag{A.11}$$

We have that:

$$|\widehat{v}|^2 = (f - \delta f)(\overline{f} - \overline{\delta f}) = |f|^2 - \overline{f}\delta f - f\overline{\delta f} + \delta f \overline{\delta f}; \tag{A.12}$$

$$\begin{aligned} &- \overline{f}\delta f - f\overline{\delta f} + \delta f \overline{\delta f} = -\overline{f}(f_{\rm appr} - \widehat{v}_{\rm appr} + \Delta_1) - f\overline{(f_{\rm appr} - \widehat{v}_{\rm appr} + \Delta_1)} + \\ &+ (f_{\rm appr} - \widehat{v}_{\rm appr} + \Delta_1)\overline{(f_{\rm appr} - \widehat{v}_{\rm appr} + \Delta_1)} = \\ &= -\overline{(f_{\rm appr} + \Delta_2)}(f_{\rm appr} - \widehat{v}_{\rm appr} + \Delta_1) - (f_{\rm appr} + \Delta_2)\overline{(f_{\rm appr} - \widehat{v}_{\rm appr} + \Delta_1)} + \\ &+ (f_{\rm appr} - \widehat{v}_{\rm appr} + \Delta_1)\overline{(f_{\rm appr} - \widehat{v}_{\rm appr} + \Delta_1)} = -|f_{\rm appr}|^2 + |\widehat{v}_{\rm appr}|^2 + \Delta_3, \end{aligned} \tag{A.13}$$

where δf is defined by (A.6), and

$$\begin{aligned} \Delta_3 &:= -\overline{\Delta_2}(f_{\rm appr} - \widehat{v}_{\rm appr} + \Delta_1) - \Delta_2\overline{(f_{\rm appr} - \widehat{v}_{\rm appr} + \Delta_1)} + \Delta_1\overline{\Delta_1} - \overline{f_{\rm appr}}(-\widehat{v}_{\rm appr} + \Delta_1) \\ &- f_{\rm appr}\overline{(-\widehat{v}_{\rm appr} + \Delta_1)} + f_{\rm appr}\overline{(-\widehat{v}_{\rm appr} + \Delta_1)} + (-\widehat{v}_{\rm appr} + \Delta_1)\overline{f_{\rm appr}} - \widehat{v}_{\rm appr}\overline{\Delta_1} - \Delta_1\overline{\widehat{v}_{\rm appr}} = \\ &= -\overline{\Delta_2}(f_{\rm appr} - \widehat{v}_{\rm appr} + \Delta_1) - \Delta_2\overline{(f_{\rm appr} - \widehat{v}_{\rm appr} + \Delta_1)} + \Delta_1\overline{\Delta_1} - \widehat{v}_{\rm appr}\overline{\Delta_1} - \Delta_1\overline{\widehat{v}_{\rm appr}}. \end{aligned} \tag{A.14}$$

From (A.14) it follows that:

$$|\Delta_3| \le 2|\Delta_2||f_{\rm appr} - \widehat{v}_{\rm appr}| + 2|\Delta_1||\Delta_2| + |\Delta_1|^2 + 2|\widehat{v}_{\rm appr}||\Delta_1|. \tag{A.15}$$

From (2.24), (A.2), (A.15) it follows that

$$|\Delta_3| \le c_6(s,D)\left(N + bE^{-\alpha} + NbE^{-\alpha-1/2}\right) bNE^{-\alpha-1/2}, \quad E^{1/2} \ge \rho_1(d,s,N). \tag{A.16}$$

Lemma 3.6 is proved.

Appendix B Proof of Theorem 3.7

Reconstruction in Born approximation. Due to the definition of u_E^1 and estimate (2.38), we have that

$$\|v - u_E^1\|_{L^\infty(D)} = \mathcal{O}(E^{-\alpha_1}),\ \text{as } E \to +\infty,\ \alpha_1 = \frac{1}{2}\frac{m-d}{m+\beta}. \tag{B.1}$$

Induction step. Let

$$\|v - u_E^j\|_{L^\infty(D)} = \mathcal{O}(E^{-\alpha_j}),\ \text{as } E \to +\infty,\ j \in \mathbb{N}. \tag{B.2}$$

We consider u_E^{j+1} defined in either Algorithm 2(A) or 2(B) with $\nu_j = 1$ and τ_j given by (3.10). To estimate $v - u_E^{j+1}$, we use Lemma 3.6 with $v + w_1$, $u_E^j + w_1$ in place of v, $v_{\rm appr}$ in case of Algorithm 2(A) and also with v itself and with u_E^j in place of $v_{\rm appr}$ in case of Algorithm 2(B). From this lemma we obtain that

$$|\widehat{v}(p) + \widehat{w}_1(p)|^2 = \Sigma_1^j(p,E) + \mathcal{O}(E^{-\alpha_j - 1/2}) \quad \text{as } E \to +\infty,\ p \in B_{2\sqrt{E}}, \tag{B.3}$$

$$|\widehat{v}(p)|^2 = \Sigma^j(p,E) + \mathcal{O}(E^{-\alpha_j - 1/2}) \quad \text{as } E \to +\infty,\ p \in B_{2\sqrt{E}}, \tag{B.4}$$

where Σ_1^j, Σ^j are defined by formulas 4 and 5 of Algorithm 2(B).

We set:

$$\Delta h^{j+1}(p,E) := |\widehat{v}(p) + \widehat{w}_1(p)|^2 - \Sigma_1^j(p,E),\ p \in B_{2\sqrt{E}},\ \text{for Algorithm 2(A);} \tag{B.5}$$

$$\Delta h^{j+1}(p,E) := |\widehat{v}(p) + \widehat{w}_1(p)|^2 - |\widehat{v}(p)|^2 - \Sigma_1^j(p,E) + \Sigma^j(p,E),\ p \in B_{2\sqrt{E}},\ \text{for Algorithm 2(B).} \tag{B.6}$$

In order to estimate $\widehat{v} - \widehat{u}_E^{j+1}$ we repeat the proofs of Theorems 5.1 and 5.2 of [41] up to the following detail:

- We replace formulas (114), (127), (116), (129) for $\Delta h(p,E)$ in [41] by formulas (B.5), (B.6), (B.3), (B.4) of the present work.

We obtain that

$$|\widehat{v}(p) - \widehat{u}_E^{j+1}(p)| = |(\overline{\mathcal{F}w_1}(p))^{-1}|\mathcal{O}(E^{-\alpha_j - 1/2}),\ p \in B_{2\tau E^{\gamma_{j+1}}},\ \gamma_{j+1} = \frac{\alpha_j + 1/2}{m+\beta}. \tag{B.7}$$

In order to estimate $v - u_E^{j+1}$ we proceed from (B.7), and repeat the proofs of Theorems 6.1 and 6.2 of [41] up to the following details:

- Formula (136) of [41] should be replaced by

$$(2 - \delta(E))\sqrt{E} = 2\tau E^{\gamma_{j+1}},\ \gamma_{j+1} = \frac{\alpha_j + 1/2}{m+\beta}, \tag{B.8}$$

- $v_{\rm appr}$ should be replaced by u_E^{j+1},
- formula (138) for $\widehat{v} - \widehat{u}_E^{j+1}$ in [41] should be replaced by (B.7).

This way provides us the following estimates:

$$|v(x) - u_E^{j+1}(x)| = \mathcal{O}(E^{-\gamma_{j+1}(m-d)}) + \mathcal{O}(E^{-\alpha_j - 1/2 + \gamma_{j+1}(d+\beta)}),\ x \in D. \tag{B.9}$$

In addition, taking into account the value of γ_{j+1} we have that, for $E \to +\infty$:

$$|v(x) - u_E^{j+1}(x)| = \mathcal{O}(E^{-\alpha_{j+1}}),\ \alpha_{j+1} = \left(\alpha_j + \frac{1}{2}\right)\frac{m-d}{m+\beta}. \tag{B.10}$$

Therefore, from the properties of arithmetico-geometric sequence for $\{\alpha_j\}$ we obtain:

$$\alpha_j = \frac{1}{2}\frac{m-d}{\beta+d}\left(1 - \left(\frac{m-d}{m+\beta}\right)^j\right),\ \forall\, j \in \mathbb{N}. \tag{B.11}$$

This completes the proof of Theorem 3.7.

References

1. A.D. Agaltsov, T. Hohage, R.G. Novikov, *An iterative approach to monochromatic phaseless inverse scattering*, Inverse Problems 35, 24001 (24 pp.) (2019)

2. A. D. Agaltsov, R.G. Novikov, *Error estimates for phaseless inverse scattering in the Born approximation at high energies*, J. Geom. Anal. (2017), https://doi.org/10.1007/s12220-017-9872-6, e-print: https://hal.archives-ouvertes.fr/hal-01303885v2

3. T. Aktosun, P. E. Sacks, *Inverse problem on the line without phase information*, Inverse Problems 14, 211–224 (1998)

4. N.V. Alexeenko, V.A. Burov, O.D. Rumyantseva, *Solution of the three-dimensional acoustical inverse scattering problem. The modified Novikov algorithm,* Acoust. Phys. 54(3), 407–419 (2008)

5. H. Ammari, Y.T. Chow, J. Zou, *Phased and phaseless domain reconstructions in the inverse scattering problem via scattering coefficients,* SIAM J. Appl. Math. 76, no. 3, 1000–1030 (2016)

6. J. A. Barceló, C. Castro, and J. M. Reyes, *Numerical approximation of the potential in the two-dimesional inverse scattering problem,* Inverse Problems, 32(1), 015006 (19pp) (2016)

7. A.H. Barnett, Ch.L. Epstein, L.F. Greengard, J.F. Magland, *Geometry of the phase retrieval problem—graveyard of algorithms* Cambridge University Press, Cambridge (2022)

8. F.A. Berezin, M.A. Shubin, *The Schrödinger Equation*, Mathematics and Its Applications, Vol. 66, Kluwer Academic, Dordrecht, 1991

9. M. Born, *Quantenmechanik der Stossvorgange*, Zeitschrift fur Physik 38 (11-12), 803-827 (1926)

10. V.A. Burov, N.V. Alekseenko, O.D. Rumyantseva, *Multifrequency generalization of the Novikov algorithm for the two-dimensional inverse scattering problem,* Acoust. Phys. 55(6), 843–856 (2009)

11. K. Chadan, P.C. Sabatier, *Inverse Problems in Quantum Scattering Theory*, 2nd edn. Springer, Berlin, 1989

12. K. Engel, B. Laasch, *The modulus of the Fourier transform on a sphere determines 3-dimensional convex polytopes*, J. Inverse Ill-Posed Probl., https://doi.org/10.1515/jiip-2020-0103

13. G. Eskin, *Lectures on Linear Partial Differential Equations*, Graduate Studies in Mathematics, Vol. 123, American Mathematical Society, 2011

14. L.D. Faddeev, *Uniqueness of the solution of the inverse scattering problem,* Vestn. Leningrad Univ. 7, 126–130 (1956) (in Russian)

15. D. Fanelli, O. Öktem, *Electron tomography: a short overview with an emphasis on the absorption potential model for the forward problem,* Inverse Problems, 24(1), 013001 (51 pp.) (2008)

16. L.D. Faddeev, S.P. Merkuriev, *Quantum Scattering Theory for Multi-particle Systems*, Mathematical Physics and Applied Mathematics, 11. Kluwer Academic Publishers Group, Dordrecht, 1993

17. A.A. Govyadinov, G.Y. Panasyuk, J.C. Schotland, *Phaseless three-dimensional optical nanoimaging*, Phys. Rev. Lett. 103, 213901 (2009)

18. P. Hähner, T. Hohage, *New stability estimates for the inverse acoustic inhomogeneous medium problem and applications,* SIAM J. Math. Anal., 33(3):670–685, (2001)

19. M. Hanke, *Regularizing properties of a truncated Newton-CG algorithm for nonlinear inverse problems*, Numer. Funct. Anal. Optim., 18:971-993, 1997.

20. T. Hohage, R.G. Novikov, *Inverse wave propagation problems without phase information*, Inverse Problems 35, 070301 (4 pp.)(2019)

21. N.E. Hurt, *Phase retrieval and zero crossings*, Kluwer Academic Publishers Group, Dordrecht (1989)

22. T. Hohage, F. Werner, *Inverse problems with Poisson data: statistical regularization theory, applications and algorithms*, Inverse Problems, 32:093001, 56, (2016)

23. O. Ivanyshyn, R. Kress, *Inverse scattering for surface impedance from phase-less far field data*, J. Comput. Phys. 230(9), 3443-3452 (2011)

24. M. Isaev, R.G. Novikov, *Hölder-logarithmic stability in Fourier synthesis*, Inverse Problems 36, 125003 (2020)

25. M. Isaev, R.G. Novikov , *Stability estimates for reconstruction from the Fourier transform on the ball*, Journal of Inverse and Ill-posed Problems, 29(3), 421-433 (2021)

26. M. Isaev, R.G. Novikov , G. V. Sabinin, *Numerical reconstruction from the Fourier transform on the ball using prolate spheroidal wave functions*, Inverse Problems, 38(10), 105002 (2022)

27. A. Jesacher, W. Harm, S. Bernet, M. Ritsch-Marte, *Quantitative single-shot imaging of complex objects using phase retrieval with a designed periphery*, Opt. Express 20, 5470–5480 (2012)

28. J. Keiner, S. Kunis, D. Potts, *Using NFFT 3—a software library for various nonequispaced fast Fourier transforms*, ACM Trans. Math. Software, 36(4), (2009)

29. M.V. Klibanov, *Phaseless inverse scattering problems in three dimensions*, SIAM J.Appl. Math. 74(2), 392-410 (2014)

30. M.V. Klibanov, N.A. Koshev, D.-L. Nguyen, L.H. Nguyen, A. Brettin, V.N. Astratov, *A numerical method to solve a phaseless coefficient inverse problem from a single measurement of experimental data*, SIAM J. Imaging Sci. 11(4), 2339-2367 (2018)

31. M.V. Klibanov, V.G. Romanov, *Reconstruction procedures for two inverse scattering problems without the phase information*, SIAM J. Appl. Math. 76(1), 178-196 (2016)

32. M.V. Klibanov, P.E. Sacks, A.V. Tikhonravov, *The phase retrieval problem*, Inverse Problems 11, 1–28 (1995)

33. B. Leshem, R. Xu, Y. Dallal, J. Miao, B. Nadler, D. Oron, N. Dudovich, O. Raz, *Direct single-shot phase retrieval from the diffraction pattern of separated objects,* Nature Communications 7(1), 1-6 (2016)

34. R. G. Novikov, *Approximate Lipschitz stability for non-overdetermined inverse scattering at fixed energy*, J. Inverse Ill-Posed Probl., 21:6, 813–823 (2013)

35. R. G. Novikov, *An iterative approach to non-overdetermined inverse scattering at fixed energy*, Sbornik: Mathematics 206(1), 120-134 (2015)

36. R. G. Novikov, *Inverse scattering without phase information*, Seminaire Laurent Schwartz - EDP et applications (2014-2015), Exp. No16, 13p

37. R. G. Novikov, *Explicit formulas and global uniqueness for phaseless inverse scattering in multidimensions*, J. Geom. Anal. 26(1), 346-359 (2016), e-print: https://hal.archives-ouvertes.fr/hal-01095750v1

38. R. G. Novikov, *Multipoint formulas for phase recovering from phaseless scattering data*, The Journal of Geometric Analysis, 31(2), 1965-1991 (2021)

39. R.G. Novikov, *Multidimensional inverse scattering for the Schrödinger equation*, In: Cerejeiras, P., Reissig, M. (eds) Mathematical Analysis, its Applications and Computation. ISAAC 2019. Springer Proceedings in Mathematics & Statistics, vol 385, pp 75-98 (2022).Springer, Cham.

40. R. G. Novikov, V. N. Sivkin, *Error estimates for phase recovering from phaseless scattering data*, Eurasian Journal of Mathematical and Computer Applications, vol. 8(1), 44–61, (2020)

41. R. G. Novikov, V. N. Sivkin, *Phaseless inverse scattering with background information*, Inverse Problems, 37(5), 055011 (2021)

42. R. G. Novikov, V. N. Sivkin, *Fixed-distance multipoint formulas for the scattering amplitude from phaseless measurements*, Inverse Problems, 38(2), 025012 (2022)

43. M.F. Perutz, *X-ray Analysis of Hemoglobin: The results suggest that a marked structural change accompanies the reaction of hemoglobin with oxygen,* Science, 140(3569), 863-869 (1963)

44. S.G. Podorov, K.M. Pavlov, D.M. Paganin, *A non-iterative reconstruction method for direct and unambiguous coherent diffractive imaging*, Optics Express, 15(16), 9954-9962 (2007)

45. V. G. Romanov, *Inverse problems without phase information that use wave interference*, Sib. Math. J. 59(3), 494-504 (2018)

46. V.G. Romanov, *Phaseless problem of determination of anisotropic conductivity in electrodynamic equations*, Dokl. Math., 104(3), 385-389 (2021)

47. Y. Shechtman, Y.C. Eldar, O. Cohen, H.N. Chapman, J. Miao, J. M. Segev, *Phase retrieval with application to optical imaging: a contemporary overview* , IEEE signal processing 32, 87–109 (2015)

48. A.S. Shurup, *Numerical comparison of iterative and functional-analytic algorithms for inverse acoustic scattering,* Eurasian Journal of Mathematical and Computer Applications **10**(1), 79-99 (2022)

49. T. Salditt, A.-L. Robisch, *Coherent X-ray Imaging,* Nanoscale Photonic Imaging (eds. T. Salditt, A. Egner, R. Luke), pp. 35–70, Springer Int'l Publishing, `https://doi.org/10.1007/978-3-030-34413-9_2` (2020)

50. G. Vainikko, *Fast Solvers of the Lippmann-Schwinger equation* Direct and Inverse Problems of Mathematical Physics (eds R.P. Gilbert, J. Kajiwara, Y.S. Xu) Kluwer, Dordrecht (2000).

51. H. Wendland, *Error estimates for interpolation by compactly supported radial basis functions of minimal degree,* J. Approx. Theory 93, 258–72 (1998)

52. X. Xu, B. Zhang, H. Zhang, *Uniqueness in inverse electromagnetic scattering problem with phaseless far–field data at a fixed frequency*, IMA Journal of Applied Mathematics 85(6), 823-839 (2020)

53. Y. Ziyang, H. Wang, *Phase retrieval with background information*, Inverse Problems 35, 054003 (20pp.) (2019)

Thorsten Hohage, Inst. Numerical and Applied Math., Univ. Göttingen, Germany
E-mail: hohage@math.uni-goettingen.de

Roman G. Novikov, CMAP, CNRS, Ecole Polytechnique, Institut Polytechnique de Paris, 91128 Palaiseau, France
& IEPT RAS, 117997 Moscow, Russia
E-mail: roman.novikov@polytechnique.edu

Vladimir N. Sivkin, CMAP, CNRS, Ecole Polytechnique, Institut Polytechnique de Paris, 91128 Palaiseau, France
& Department of Mechanics and Mathematics, Lomonosov MSU & Center of Fundamental and Applied Mathematics, Lomonosov MSU, Moscow, 119991, Russia
E-mail: sivkin96@yandex.ru